

Attack Detection in Sensor Network Target Localization Systems with Quantized Data

Jiangfan Zhang, *Member, IEEE*, Xiaodong Wang, *Fellow, IEEE*, Rick S. Blum, *Fellow, IEEE*,
and Lance M. Kaplan, *Fellow, IEEE*

Abstract

We consider a sensor network focused on target localization, where sensors measure the signal strength emitted from the target. Each measurement is quantized to one bit and sent to the fusion center. A general attack is considered at some sensors that attempts to cause the fusion center to produce an inaccurate estimation of the target location with a large mean-square-error. The attack is a combination of man-in-the-middle, hacking, and spoofing attacks that can effectively change both signals going into and coming out of the sensor nodes in a realistic manner. We show that the essential effect of attacks is to alter the estimated distance between the target and each attacked sensor to a different extent, giving rise to a geometric inconsistency among the attacked and unattacked sensors. Hence, with the help of two secure sensors, a class of detectors are proposed to detect the attacked sensors by scrutinizing the existence of the geometric inconsistency. We show that the false alarm and miss probabilities of the proposed detectors decrease exponentially as the number of measurement samples increases, which implies that for sufficiently large number of samples, the proposed detectors can identify the attacked and unattacked sensors with any required accuracy.

Index Terms

Target localization, attack detection, spoofing attack, man-in-the-middle attack, malfunction, sensor network, large deviations theory.

I. INTRODUCTION

Sensor networks find wide applications ranging from inexpensive commercial systems to complex military and homeland defense surveillance systems and have seen ever growing interest in recent years [1]. One important application of sensor networks is to estimate the location of a target in a region of interest (ROI) [2]–[4]. Recent technological advances in digital wireless communications and digital

electronics have led to the dominance of digital transmission and processing using quantized data in such systems. Hence, a great deal of attention has focused on target localization in sensor networks using quantized data, see [5]–[7] for instance.

Typically, large-scale sensor networks are comprised of low-cost and spatially distributed sensor nodes with limited battery capacity and low computing power, which makes the system vulnerable to cyberattacks by adversaries. This has led to a vast interest in studying the vulnerability of sensor networks in various applications and from different perspectives, see [8]–[15] and the references therein. Depending on the place where the attack is launched, there are generally three categories of attacks in sensor networks, namely spoofing attacks, hacking attacks, and man-in-the-middle attacks (MiMA). To be specific, the spoofing attack changes the phenomenon observed by the attacked sensors and tampers with the observations coming into the sensors. For example, data-injection attack is one type of spoofing attack [10]. The hacking attack aims at hacking into the sensors, modifying the hardware, and/or reprogramming the devices, with the goal of disrupting the data processing in the attacked sensors. Note that malfunctions of sensors can also be considered as hacking attacks. The MiMA takes place between the sensors and a fusion center (FC), which maliciously falsifies the data transmitted from the attacked sensors to the FC, see [7], [11], [12] for instance. The main goal of the adversaries is to undermine the sensor network and render the FC to reach an inaccurate estimate of the target location in terms of large mean-square estimation error. A simple and intuitive method to combat the attacks is to identify the attacked sensors so that the FC can either discard data from these sensors, or make use of attacked data to improve its estimate of the target location via jointly estimating the target location and the attacks [11], [12], [15].

A. Summary of Results and Main Contributions

In this paper, we consider a sensor network containing two widely separated secure sensors which have a very high level of security and thereby are guaranteed to be tamper-proof. The rest of sensors are unsecure, which are subject to arbitrary forms of attacks. In practice, the two secure sensors can be well protected, built with powerful chips, and supplied with sufficient power, thereby highly sophisticated encryption algorithms and security procedures can be implemented.

This paper aims at developing a general detection approach which does not rely on the form of the attacks or attack parameters, to identify the attacked sensors in the sensor network with provable detection performance guarantee. It is worth mentioning that the problem of attack detection in target localization systems is difficult, since the statistical model of sensor data depend on the target location and the attack strategy which are both unknown to the FC. By exploring the impact of the attacks on the statistical

model of the sensor data, we reveal that the essential effect of attacks is to alter the estimated distance between the target and each attacked sensor to a different extent, giving rise to a geometric inconsistency among the attacked and unattacked sensors. Motivated by this fact, a class of detectors are proposed to detect the attacked sensors via scrutinizing the existence of the geometric inconsistency. To be specific, a naive maximum likelihood estimator (NMLE), the MLE formulated under the assumption of no attack, is first employed to estimate the distance between the target and each sensor. For each unsecure sensor, a circle is generated which is centered at the sensor with radius equal to the NMLE of its distance to the target. For each of the two secure sensors, a ring with some constant width is generated. This ring is centered at the sensor and is bisected by a circle with radius equal to the NMLE of the distance from the sensor to the target. If the circle of an unsecure sensor passes through the common area of the two rings, the sensor is declared unattacked; otherwise, we declare that it is under attack. A thorough performance analysis is carried out for the proposed detectors, showing that the false alarm and miss probabilities decrease exponentially as the number of data samples at each sensor grows, which implies that if for a sufficiently large number of samples, the proposed detectors can identify the attacked sensors with an arbitrary level of accuracy.

B. Related Works

With the proliferation of sensor network applications, there is an increasing concern about the security of sensor networks, see [8], [9], [16]–[19] for instance. Most existing works on the security in sensor network target localization systems only consider analog measurements. However, for a typical sensor network with limited resources, it is desirable that only quantized data is transmitted from sensors to the FC [5]–[7]. Moreover, there is a lack of theoretical performance analysis of attack detection strategies.

Attack detection in the context of target localization with quantized data has not been well investigated in the literature. In [7], a specific attack model is considered and a practical approach is proposed to detect attacks in target localization systems. In particular, several secure sensors are employed to provide a coarse estimate of the target location, and then the expected behaviors of attacked and unattacked sensors are calculated based on the coarse estimate and the attack model. This method is based on heuristic and there is no detection performance guarantee. In our proposed approach, the estimate of the target location is not required, and moreover, the attack detection performance is rigorously investigated, which demonstrates that any identification accuracy can be achieved if the number of data samples is sufficiently large. In addition, the approach in [7] requires the knowledge of the statistical model of the attack, which is not required by our proposed approach.

The remainder of the paper is organized as follows. Section II describes the system and adversary model. In Section III, a class of detectors are proposed to identify the attacked sensors in the sensor network. Section IV investigates the performance of the proposed detectors. In Section V, several numerical results are provided to corroborate our theoretical analysis. Finally, Section VI provides our conclusions.

II. SYSTEM AND ADVERSARY MODELS

In this section, the system and general attack models are introduced. We also demonstrate how the general attack model relates to some popular forms of attacks in practice.

A. System Model

Consider a sensor network consisting of N sensors and a FC to estimate the location of a target at $\boldsymbol{\theta}_T = [x_T, y_T]$, where x_T and y_T denote the coordinates of the target location on the two-dimensional plane. For the j -th sensor, we use $\boldsymbol{\theta}_j = [x_j, y_j]$ to denote its location. Besides the N sensors, there also exist two secure sensors in the sensor network which are labeled as the $(N+1)$ -th and $(N+2)$ -th sensors, respectively. These two secure sensors are well protected and thereby are guaranteed to be tamper proof, while the other N sensors are unsecure, which are subject to threat from adversaries. We assume that the signal radiated from the target obeys an isotropic power attenuation model, and each sensor observes K data samples. The k -th data sample at the j -th sensor is described as

$$s_{jk} = P_0 \left(\frac{D_0}{D_j} \right)^\gamma + n_{jk}, \quad j = 1, 2, \dots, N+2, \quad (1)$$

where the distance D_j between the j -th sensor and the target is defined by

$$D_j \triangleq \|\boldsymbol{\theta}_j - \boldsymbol{\theta}_T\| = \sqrt{(x_j - x_T)^2 + (y_j - y_T)^2}, \quad j = 1, 2, \dots, N+2, \quad (2)$$

the quantity P_0 is the power measured at a reference distance D_0 , γ is the path-loss exponent, and n_{jk} denotes the additive noise sample with probability density function (pdf) $f_j(n_{jk})$.

We assume that P_0 , D_0 , γ , $\{f_j(\cdot)\}_{j=1}^{N+2}$, and $\{\boldsymbol{\theta}_j\}_{j=1}^{N+2}$ are known to the FC. Moreover, we assume $\{n_{jk}\}$ are independent, and for each j , $\{n_{jk}\}_{k=1}^K$ is an identically distributed sequence. In addition, we assume that the target stays in a specified ROI \mathcal{A} where no sensor exists. By defining

$$D_L \triangleq \min_{j=1,2,\dots,N+2} \inf_{\boldsymbol{\theta} \in \mathcal{A}} \|\boldsymbol{\theta}_j - \boldsymbol{\theta}\| > 0, \quad (3)$$

$$\text{and } D_U \triangleq \max_{j=1,2,\dots,N+2} \sup_{\boldsymbol{\theta} \in \mathcal{A}} \|\boldsymbol{\theta}_j - \boldsymbol{\theta}\| < \infty, \quad (4)$$

we know that for any $j \in \{1, 2, \dots, N + 2\}$,

$$D_j \in [D_L, D_U]. \quad (5)$$

Regarding the secure sensors and the ROI \mathcal{A} , we make the following assumption.

Assumption 1: The secure sensors are widely separated so that

$$D_S \triangleq \|\boldsymbol{\theta}_{N+1} - \boldsymbol{\theta}_{N+2}\| > D_U - D_L + 2\Upsilon_1 \quad (6)$$

for some positive constant Υ_1 . In addition, the ROI \mathcal{A} is contained in one of the two half spaces produced by dividing the whole space by the line passing through the two secure sensors. By the triangle inequality of sides, we assume

$$\inf_{\boldsymbol{\theta}_T \in \mathcal{A}} \{D_{N+1} + D_{N+2}\} > D_S + 2\Upsilon_2 \quad (7)$$

for some positive constant Υ_2 .

Due to the low-rate communication constraint between the sensors and the FC, each sensor j quantizes its sample s_{jk} to one bit and then transmits the bit to the FC. For simplicity, we assume that the sensors employ the following threshold quantizers $\{\mathcal{Q}_j\}_{j=1}^{N+2}$

$$u_{jk} = \mathcal{Q}_j(s_{jk}) \triangleq \mathbb{1}\{s_{jk} \in (\tau_j, \infty)\}, \quad j = 1, 2, \dots, N + 2, \quad k = 1, 2, \dots, K, \quad (8)$$

where τ_j is the threshold employed at the j -th sensor and we assume that the thresholds $\{\tau_j\}_{j=1}^{N+2}$ are known to the FC.

Using (1) and (8), define

$$p_j(\boldsymbol{\theta}_T) \triangleq \Pr(u_{jk} = 0 | \boldsymbol{\theta}_T) = F_j\left(\tau_j - P_0\left(\frac{D_0}{D_j}\right)^\gamma\right), \quad (9)$$

where $F_j(x) \triangleq \int_{-\infty}^x f_j(t) dt$. By employing (5) and (9), we can define

$$\rho_j^{(L)} \triangleq \inf_{\boldsymbol{\theta} \in \mathcal{A}} p_j(\boldsymbol{\theta}) = F_j\left(\tau_j - P_0\left(\frac{D_0}{D_L}\right)^\gamma\right), \quad (10)$$

$$\rho_j^{(U)} \triangleq \sup_{\boldsymbol{\theta} \in \mathcal{A}} p_j(\boldsymbol{\theta}) = F_j\left(\tau_j - P_0\left(\frac{D_0}{D_U}\right)^\gamma\right), \quad (11)$$

and hence,

$$p_j(\boldsymbol{\theta}_T) \in \left[\rho_j^{(L)}, \rho_j^{(U)}\right], \quad j = 1, 2, \dots, N + 2. \quad (12)$$

We assume that $f_j(x)$ is continuous, and $F_j^{-1}(x)$ exists and is differentiable over the open interval $(0, 1)$ for each j . Noticing that $\frac{\partial F_j^{-1}(x)}{\partial x} = [f_j(F_j^{-1}(x))]^{-1}$, the differentiability of $F_j^{-1}(x)$ implies $0 < f_j(x) < \infty$ over $\{x | F_j(x) \in (0, 1)\}$, and therefore, $F_j(x)$ is strictly increasing over $\{x | F_j(x) \in (0, 1)\}$.

It is clear that if there exists some $\boldsymbol{\theta} \in \mathcal{A}$ such that

$$\tau_j - P_0 \left(\frac{D_0}{\|\boldsymbol{\theta}_j - \boldsymbol{\theta}\|} \right)^\gamma \notin \text{supp}(f_j) \triangleq \{x | f_j(x) \neq 0\}, \quad (13)$$

then $F_j(\tau_j - P_0(\frac{D_0}{\|\boldsymbol{\theta}_j - \boldsymbol{\theta}\|})^\gamma) = 0$ or 1 , and hence, the quantized data from the j -th sensor is useless in estimating $\boldsymbol{\theta}$. To this end, we assume that the quantizers are well designed, and thereby τ_j , D_L and D_U satisfy

$$\inf \{\text{supp}(f_j)\} < \tau_j - P_0 \left(\frac{D_0}{D_U} \right)^\gamma < \tau_j - P_0 \left(\frac{D_0}{D_L} \right)^\gamma < \sup \{\text{supp}(f_j)\}, \quad (14)$$

which yields

$$0 < F_j \left(\tau_j - P_0 \left(\frac{D_0}{D_L} \right)^\gamma \right) < F_j \left(\tau_j - P_0 \left(\frac{D_0}{D_U} \right)^\gamma \right) < F_j(\tau_j) \leq 1, \quad j = 1, 2, \dots, N + 2, \quad (15)$$

since $F_j(\cdot)$ is strictly increasing, from (10) and (11), we know

$$0 < \rho_j^{(L)} < \rho_j^{(U)} < F_j(\tau_j) \leq 1. \quad (16)$$

B. Adversary Model

We consider a general attack model which brings about a change in the statistical model of u_{jk} . Let \mathcal{U} and \mathcal{V} denote the set of unattacked and attacked sensors, respectively.

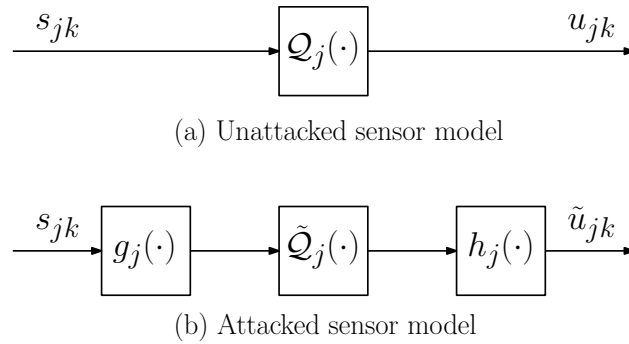


Fig. 1: Unattacked and attacked sensor models.

In general, if $j \in \mathcal{V}$, three types of possible attacks can affect the j -th sensor, which are illustrated in Fig. 1 (b). First, the adversaries can tamper with the observations $\{s_{jk}\}_{k=1}^K$. Such attacks are called spoofing attacks, which can be represented by a mapping $g_j(\cdot)$. The second type of attack which we call hacking, aims at modifying the sensor hardware and/or software, and thereby modifying the quantizer $Q_j(\cdot)$ to $\tilde{Q}_j(\cdot)$ in the attacked sensors as shown in Fig. 1 (b). The last type of possible attack occurs between the sensors and the FC, which is referred to as man-in-the-middle attacks (MiMA). The MiMA

can be described by a mapping $h_j(\cdot)$ that modifies the quantized data before it arrives at the FC. Therefore, the post attack quantized data can be generally expressed as

$$\tilde{u}_{jk} = h_j \left(\tilde{\mathcal{Q}}_j (g_j (s_{jk})) \right). \quad (17)$$

With regard to the alphabet set of \tilde{u}_{jk} , we make the following assumption.

Assumption 2: We assume that if $j \in \mathcal{V}$, then the alphabet set of \tilde{u}_{jk} is still $\{0, 1\}$. Otherwise, the detection of attacks is trivial.

Define

$$\tilde{p}_j(\boldsymbol{\theta}_T) \triangleq \Pr(\tilde{u}_{jk} = 0 | \boldsymbol{\theta}_T) = p_j(\boldsymbol{\theta}_T) + \Psi_j, \quad j = 1, 2, \dots, N, \quad (18)$$

where the quantity Ψ_j represents the impact of the attacks on the statistical model of the data. Clearly, if $\Psi_j = 0$, then we can ignore the corresponding attack, since it is ineffective from the perspective of the FC. Hence, without loss of generality, if $j \in \mathcal{V}$, then we assume $\Psi_j \neq 0$, while if $j \in \mathcal{U}$, then $\Psi_j = 0$.

To illustrate (18) in a concrete way, we take the MiMA as an example. Under a class of MiMAs [7], [11], [12], the quantized data u_{jk} is flipped with probability $\psi_{j,i}$ if $u_{jk} = i$ for $i \in \{0, 1\}$, i.e., if the j -th sensor is attacked,

$$\begin{cases} \Pr(\tilde{u}_{jk} = 1 | u_{jk} = 0) = \psi_{j,0}, \\ \Pr(\tilde{u}_{jk} = 0 | u_{jk} = 1) = \psi_{j,1}, \end{cases} \quad (19)$$

where $\psi_{j,i} \in [0, 1]$. Using (19), we have

$$\tilde{p}_j(\boldsymbol{\theta}_T) = (1 - \psi_{j,0} - \psi_{j,1}) p_j(\boldsymbol{\theta}_T) + \psi_{j,0}, \quad (20)$$

$$\text{and} \quad \Psi_j = \psi_{j,0} - (\psi_{j,0} + \psi_{j,1}) p_j(\boldsymbol{\theta}_T). \quad (21)$$

Besides the man-in-the-middle attacks, the spoofing attacks can also be shown to agree with (18) [8], [9], [15].

From a practical point of view, the following assumptions on the attacks are made throughout this paper.

Assumption 3:

- 1) *Subtle Attacks.* By the strong law of large numbers, we know that as $K \rightarrow \infty$, $\frac{1}{K} \sum_{k=1}^K (1 - \tilde{u}_{jk}) \rightarrow \tilde{p}_j(\boldsymbol{\theta}_T)$ almost surely. Thus, if $\tilde{p}_j(\boldsymbol{\theta}_T) \notin [\rho_j^{(L)}, \rho_j^{(U)}]$, then with sufficient observations, the attack against the j -th sensor can be detected at the FC by checking whether $\frac{1}{K} \sum_{k=1}^K (1 - \tilde{u}_{jk})$ is in the range $[\rho_j^{(L)}, \rho_j^{(U)}]$. For this reason, in order to reduce the possibility of being detected, the adversaries should ensure

$$\tilde{p}_j(\boldsymbol{\theta}_T) \in \left[\rho_j^{(L)}, \rho_j^{(U)} \right], \quad j \in \mathcal{V}. \quad (22)$$

2) *Significant Attacks*. In order to bring about sufficient impact on the statistical characterization of the bits from the attacked sensors, every adversary is required to guarantee a minimum distortion, i.e.,

$$|\Psi_j| > \kappa, \quad j \in \mathcal{V}, \quad (23)$$

for some positive constant κ . Otherwise, the attacks can be ignored.

Our problem is to design an efficient strategy for the FC to identify the attacked sensors, based on the binary observations it receives from all sensors, and to provide a performance analysis on the proposed attack detection strategy.

III. ATTACK DETECTORS BASED ON NAIVE MAXIMUM LIKELIHOOD ESTIMATOR

In this section, we first show that by employing a naive maximum likelihood estimator (NMLE), a geometric inconsistency among each attacked sensor and other unattacked sensors can be utilized to distinguish between the attacked and unattacked ones. Then, a class of detectors which are based on the NMLE are proposed to detect the attacks in the sensor network.

A. Naive Maximum Likelihood Estimator and Geometric Inconsistency

For any j , from (9) and by employing the existence of $F_j^{-1}(x)$, we can obtain

$$D_j = D_0 P_0^{\frac{1}{\gamma}} \left[\tau_j - F_j^{-1}(p_j(\boldsymbol{\theta}_T)) \right]^{-\frac{1}{\gamma}}. \quad (24)$$

Then the NMLE, which is the MLE under the assumption of no attack, of D_j is given by

$$\widehat{D}_j^{(K)} = D_0 P_0^{\frac{1}{\gamma}} \left[\tau_j - F_j^{-1}(\xi_j^{(K)}) \right]^{-\frac{1}{\gamma}}, \quad (25)$$

$$\text{where } \xi_j^{(K)} \triangleq \frac{1}{K} \sum_{k=1}^K (1 - \tilde{u}_{jk}). \quad (26)$$

Furthermore, define

$$\widetilde{D}_j \triangleq D_0 P_0^{\frac{1}{\gamma}} \left[\tau_j - F_j^{-1}(\tilde{p}_j(\boldsymbol{\theta}_T)) \right]^{-\frac{1}{\gamma}}. \quad (27)$$

It is seen from (27) that \widetilde{D}_j is a monotonic function of $\tilde{p}_j(\boldsymbol{\theta}_T)$, and since from (23), we know $\tilde{p}_j(\boldsymbol{\theta}_T) \neq p_j(\boldsymbol{\theta}_T)$, we have $\widetilde{D}_j \neq D_j$. What's more, by the strong law of large numbers, we know

$$\widehat{D}_j^{(K)} \rightarrow \begin{cases} D_j, & \text{if } j \in \mathcal{U} \\ \widetilde{D}_j, & \text{if } j \in \mathcal{V} \end{cases} \quad \text{almost surely, as } K \rightarrow \infty. \quad (28)$$

This implies that, from the perspective of the NMLE, if $j \in \mathcal{V}$, the essential effect of the attack is a falsification of the distance D_j between the target and the j -th sensor to some different \widetilde{D}_j . This gives

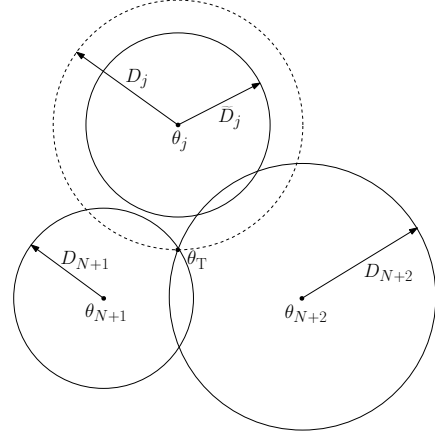
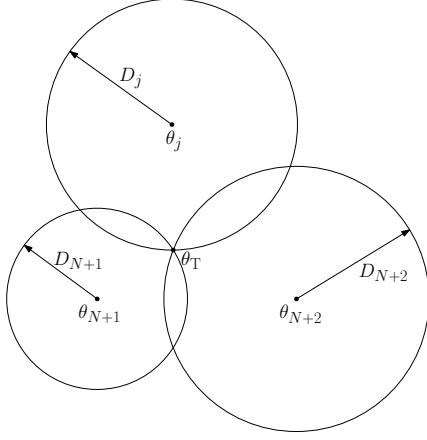


Fig. 2: Geometric consistency among the j -th, $(N + 1)$ -th and $(N + 2)$ -th sensors when $j \in \mathcal{U}$. Fig. 3: Geometric inconsistency among the j -th, $(N + 1)$ -th and $(N + 2)$ -th sensors when $j \in \mathcal{V}$.

rise to a geometric inconsistency between the j -th sensor and the two secure sensors, which is illustrated in terms of the difference between Fig. 2 and Fig. 3. Specifically, if $j \in \mathcal{U}$, as illustrated in Fig. 2, the three circles centered at the j -th, $(N + 1)$ -th and $(N + 2)$ -th sensors and with radii D_j , D_{N+1} and D_{N+2} , respectively, intersect at the point θ_T ; while if $j \in \mathcal{V}$, then the three circles do not intersect at θ_T as illustrated in Fig. 3.

Motivated by this fact, consider three circles centered at the j -th, $(N + 1)$ -th and $(N + 2)$ -th sensors and with radii $\widehat{D}_j^{(K)}$, $\widehat{D}_{N+1}^{(K)}$ and $\widehat{D}_{N+2}^{(K)}$, respectively. If $j \in \mathcal{V}$, then from (28), we know that with sufficiently large K and Assumption 3, it is impossible for these three circles to intersect at a common point. This observation forms the basis of the proposed attack detection strategy.

B. Attack Detection Strategy

In order to mathematically formulate the attack detector, we first define three geometric shapes. According to Assumption 1, the ROI \mathcal{A} is contained in one of the two half spaces produced by dividing the whole space by the line passing through the two secure sensors. We use \mathcal{S} to represent this half space. Let $\mathcal{C}(\theta_0, R)$ denote the intersection of \mathcal{S} and the circle centered at θ_0 and with radius R , i.e.,

$$\mathcal{C}(\theta_0, R) \triangleq \{\theta \in \mathcal{S} \mid \|\theta - \theta_0\| = R\}, \quad (29)$$

which is illustrated by the blue curve in Fig. 4. Let $\mathcal{R}(\theta_0, R, \delta)$ denote the intersection of \mathcal{S} and the ring centered at θ_0 , with radius R and width δ , i.e.,

$$\mathcal{R}(\theta_0, R, \delta) \triangleq \{\theta \in \mathcal{S} \mid R - \delta \leq \|\theta - \theta_0\| \leq R + \delta\}. \quad (30)$$

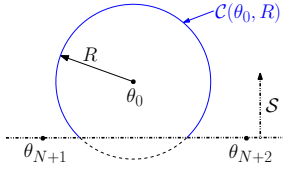


Fig. 4: Geometric illustration of $\mathcal{C}(\boldsymbol{\theta}_0, R)$.

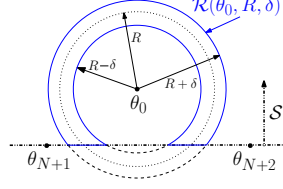


Fig. 5: Geometric illustration of $\mathcal{R}(\boldsymbol{\theta}_0, R, \delta)$.

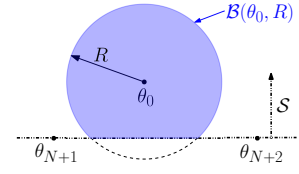


Fig. 6: Geometric illustration of $\mathcal{B}(\boldsymbol{\theta}_0, R)$.

The region enclosed by the blue boundary in Fig. 5 depicts an example of $\mathcal{R}(\boldsymbol{\theta}_0, R, \delta)$. Let $\mathcal{B}(\boldsymbol{\theta}_0, R)$ denote the intersection of \mathcal{S} and the ball centered at $\boldsymbol{\theta}_0$ and with radius R , i.e.,

$$\mathcal{B}(\boldsymbol{\theta}_0, R) \triangleq \{\boldsymbol{\theta} \in \mathcal{S} \mid \|\boldsymbol{\theta} - \boldsymbol{\theta}_0\| \leq R\}. \quad (31)$$

which is the blue region in Fig. 6.

It is worth mentioning that even though $j \in \mathcal{U}$, due to the estimation error with finite K , the three circles centered at the j -th, $(N+1)$ -th and $(N+2)$ -th sensors and with radii $\widehat{D}_j^{(K)}$, $\widehat{D}_{N+1}^{(K)}$ and $\widehat{D}_{N+2}^{(K)}$, respectively, typically will not intersect at a common point. Thus, for finite K , checking the geometric inconsistency among $\mathcal{C}(\boldsymbol{\theta}_j, \widehat{D}_j^{(K)})$, $\mathcal{C}(\boldsymbol{\theta}_{N+1}, \widehat{D}_{N+1}^{(K)})$ and $\mathcal{C}(\boldsymbol{\theta}_{N+2}, \widehat{D}_{N+2}^{(K)})$ cannot reliably tell whether the j -th sensor is unattacked or not. To overcome this, we replace $\mathcal{C}(\boldsymbol{\theta}_{N+1}, \widehat{D}_{N+1}^{(K)})$ and $\mathcal{C}(\boldsymbol{\theta}_{N+2}, \widehat{D}_{N+2}^{(K)})$ with $\mathcal{R}(\boldsymbol{\theta}_{N+1}, \widehat{D}_{N+1}^{(K)}, \delta)$ and $\mathcal{R}(\boldsymbol{\theta}_{N+2}, \widehat{D}_{N+2}^{(K)}, \delta)$ for some δ , respectively, and scrutinize whether $\mathcal{C}(\boldsymbol{\theta}_j, \widehat{D}_j^{(K)})$ pass through the common area of $\mathcal{R}(\boldsymbol{\theta}_{N+1}, \widehat{D}_{N+1}^{(K)}, \delta)$ and $\mathcal{R}(\boldsymbol{\theta}_{N+2}, \widehat{D}_{N+2}^{(K)}, \delta)$ instead.

To be specific, for the j -th sensor, $j = 1, 2, \dots, N$, we consider the following hypothesis testing problem

$$\begin{cases} \mathcal{H}_0 : j \in \mathcal{U} \\ \mathcal{H}_1 : j \in \mathcal{V} \end{cases} \quad (32)$$

and a class of detectors

$$\varpi_j(\delta) = \begin{cases} 0, & \text{if } \mathcal{C}(\boldsymbol{\theta}_j, \widehat{D}_j^{(K)}) \cap \left[\bigcap_{i=1}^2 \mathcal{R}(\boldsymbol{\theta}_{N+i}, \widehat{D}_{N+i}^{(K)}, \delta) \right] \neq \emptyset, \\ 1, & \text{if } \mathcal{C}(\boldsymbol{\theta}_j, \widehat{D}_j^{(K)}) \cap \left[\bigcap_{i=1}^2 \mathcal{R}(\boldsymbol{\theta}_{N+i}, \widehat{D}_{N+i}^{(K)}, \delta) \right] = \emptyset, \end{cases} \quad (33)$$

for some constant δ , where $\widehat{D}_j^{(K)}$ is defined in (25).

The geometric illustration of the proposed detector in (33) is depicted in Fig. 7, where the region enclosed by the red curves is the common area of $\mathcal{R}(\boldsymbol{\theta}_{N+1}, \widehat{D}_{N+1}^{(K)}, \delta)$ and $\mathcal{R}(\boldsymbol{\theta}_{N+2}, \widehat{D}_{N+2}^{(K)}, \delta)$ which plays an important role in the attack detection process. It is worth noticing that the center of this common area is determined by two random variables $\widehat{D}_{N+1}^{(K)}$ and $\widehat{D}_{N+2}^{(K)}$, and thereby is randomly located. To this

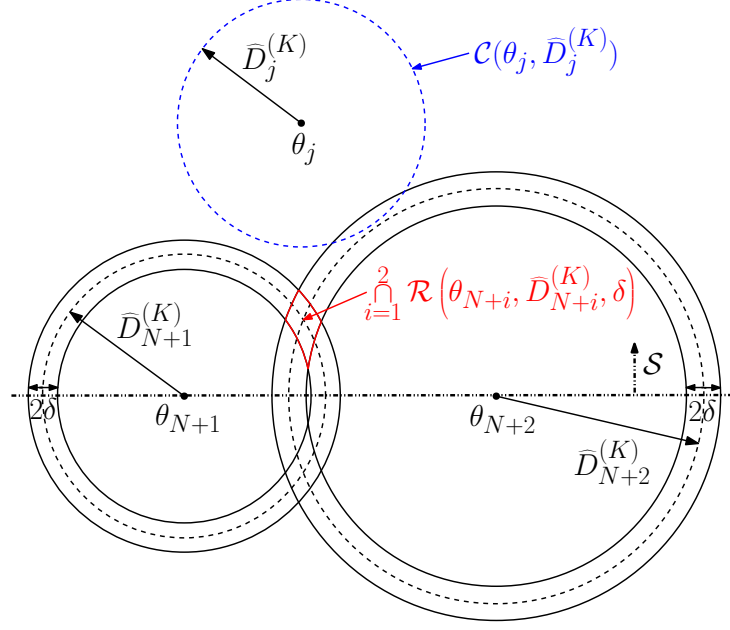


Fig. 7: Geometric illustration of the proposed detectors.

end, this common area may not cover the true target location θ_T . In addition, the size of the common area of $\mathcal{R}(\theta_{N+1}, \widehat{D}_{N+1}^{(K)}, \delta)$ and $\mathcal{R}(\theta_{N+2}, \widehat{D}_{N+2}^{(K)}, \delta)$ depends on the parameter δ which impacts the false alarm and miss probabilities of the proposed detector.

IV. PERFORMANCE ANALYSIS OF THE PROPOSED DETECTOR

In this section, the detection performance of the proposed detector in (33) is investigated. We will show that the false alarm and miss probabilities of the proposed detector decay exponentially fast as the number of data samples at each sensor increases.

To start with, we provide the following lemma regarding the lower and upper bounds on the common area of $\mathcal{R}(\theta_{N+1}, D_{N+1}, \delta)$ and $\mathcal{R}(\theta_{N+2}, D_{N+2}, \delta)$.

Lemma 1: If

$$\delta < \Upsilon \triangleq \min\{\Upsilon_1, \Upsilon_2\}, \quad (34)$$

then

$$\sup_{\theta \in \bigcap_{i=1}^2 \mathcal{R}(\theta_{N+i}, \widehat{D}_{N+i}^{(K)}, \delta)} \|\theta - \theta_T\| < \Phi(\delta) \triangleq (2D_U + \Upsilon)^{\frac{1}{2}} \left[\frac{2D_U + \Upsilon}{D_S} \left(\frac{\Upsilon}{D_S} + 1 \right) + 2 \right]^{\frac{1}{2}} \sqrt{\delta}, \quad (35)$$

which implies

$$\mathcal{B}(\theta_T, \delta) \subseteq \bigcap_{i=1}^2 \mathcal{R}(\theta_{N+i}, \widehat{D}_{N+i}^{(K)}, \delta) \subseteq \mathcal{B}(\theta_T, \Phi(\delta)). \quad (36)$$

Proof: Refer to Appendix A. ■

As demonstrated by Lemma 1, the common area of $\mathcal{R}(\boldsymbol{\theta}_{N+1}, D_{N+1}, \delta)$ and $\mathcal{R}(\boldsymbol{\theta}_{N+2}, D_{N+2}, \delta)$ can be bounded by two balls from below and above. Moreover, the radii of these two balls are both increasing functions of the given δ . It will be shown later that by employing the two balls to approximate the irregular area $\cap_{i=1}^2 \mathcal{R}(\boldsymbol{\theta}_{N+i}, \widehat{D}_{N+i}^{(K)}, \delta)$ from below and above, the detection performance analysis of the proposed detector in (33) can be considerably facilitated.

A. Upper Bound on False Alarm Probability

From (33), the false alarm and miss probabilities of the proposed detector are given by $\mathbb{P}_0(\varpi_j(\delta) = 1)$ and $\mathbb{P}_1(\varpi_j(\delta) = 0)$, respectively, where \mathbb{P}_i denotes the probability measure under hypothesis \mathcal{H}_i .

Let \mathcal{E}_i denote the event

$$\mathcal{E}_i \triangleq \left\{ \left| \widehat{D}_{N+i}^{(K)} - D_{N+i} \right| < \frac{1}{2}\delta \right\}, \quad i = 1, 2, \quad (37)$$

and \mathcal{E}_i^C denotes the complement of the event \mathcal{E}_i . The false alarm probability of the detector in (33) can be expressed as

$$\begin{aligned} \mathbb{P}_0(\varpi_j(\delta) = 1) &= \mathbb{P}_0 \left(\mathcal{C}(\boldsymbol{\theta}_j, \widehat{D}_j^{(K)}) \cap \left[\bigcap_{i=1}^2 \mathcal{R}(\boldsymbol{\theta}_{N+i}, \widehat{D}_{N+i}^{(K)}, \delta) \right] = \emptyset \right) \\ &= \mathbb{P}_0 \left(\left\{ \mathcal{C}(\boldsymbol{\theta}_j, \widehat{D}_j^{(K)}) \cap \left[\bigcap_{i=1}^2 \mathcal{R}(\boldsymbol{\theta}_{N+i}, \widehat{D}_{N+i}^{(K)}, \delta) \right] = \emptyset \right\} \cap (\mathcal{E}_1 \cap \mathcal{E}_2) \right) \\ &\quad + \mathbb{P}_0 \left(\left\{ \mathcal{C}(\boldsymbol{\theta}_j, \widehat{D}_j^{(K)}) \cap \left[\bigcap_{i=1}^2 \mathcal{R}(\boldsymbol{\theta}_{N+i}, \widehat{D}_{N+i}^{(K)}, \delta) \right] = \emptyset \right\} \cap (\mathcal{E}_1^C \cup \mathcal{E}_2^C) \right). \end{aligned} \quad (38)$$

Note that \mathcal{E}_i implies that

$$\mathcal{R}\left(\boldsymbol{\theta}_{N+i}, D_{N+i}, \frac{1}{2}\delta\right) \subseteq \mathcal{R}\left(\boldsymbol{\theta}_{N+i}, \widehat{D}_{N+i}^{(K)}, \delta\right), \quad (39)$$

and hence, from (38), we can obtain

$$\begin{aligned} \mathbb{P}_0(\varpi_j(\delta) = 1) &\leq \mathbb{P}_0 \left(\left\{ \mathcal{C}(\boldsymbol{\theta}_j, \widehat{D}_j^{(K)}) \cap \left[\bigcap_{i=1}^2 \mathcal{R}\left(\boldsymbol{\theta}_{N+i}, D_{N+i}, \frac{1}{2}\delta\right) \right] = \emptyset \right\} \cap (\mathcal{E}_1 \cap \mathcal{E}_2) \right) \\ &\quad + \mathbb{P}_0 \left(\left\{ \mathcal{C}(\boldsymbol{\theta}_j, \widehat{D}_j^{(K)}) \cap \left[\bigcap_{i=1}^2 \mathcal{R}\left(\boldsymbol{\theta}_{N+i}, \widehat{D}_{N+i}^{(K)}, \delta\right) \right] = \emptyset \right\} \cap (\mathcal{E}_1^C \cup \mathcal{E}_2^C) \right) \\ &\leq \mathbb{P}_0 \left(\mathcal{C}(\boldsymbol{\theta}_j, \widehat{D}_j^{(K)}) \cap \left[\bigcap_{i=1}^2 \mathcal{R}\left(\boldsymbol{\theta}_{N+i}, D_{N+i}, \frac{1}{2}\delta\right) \right] = \emptyset \right) + \mathbb{P}_0(\mathcal{E}_1^C \cup \mathcal{E}_2^C) \end{aligned} \quad (40)$$

$$\leq \mathbb{P}_0 \left(\mathcal{C}(\boldsymbol{\theta}_j, \widehat{D}_j^{(K)}) \cap \left[\bigcap_{i=1}^2 \mathcal{R}\left(\boldsymbol{\theta}_{N+i}, D_{N+i}, \frac{1}{2}\delta\right) \right] = \emptyset \right) + \mathbb{P}_0(\mathcal{E}_1^C) + \mathbb{P}_0(\mathcal{E}_2^C), \quad (41)$$

where (40) is due to the fact that $\mathbb{P}_0(\mathcal{E} \cap \mathcal{F}) \leq \mathbb{P}_0(\mathcal{E})$ for any two events \mathcal{E} and \mathcal{F} . Moreover, from Lemma 1, we know

$$\mathcal{B}\left(\boldsymbol{\theta}_T, \frac{1}{2}\delta\right) \subseteq \bigcap_{i=1}^2 \mathcal{R}\left(\boldsymbol{\theta}_{N+i}, D_{N+i}, \frac{1}{2}\delta\right), \quad (42)$$

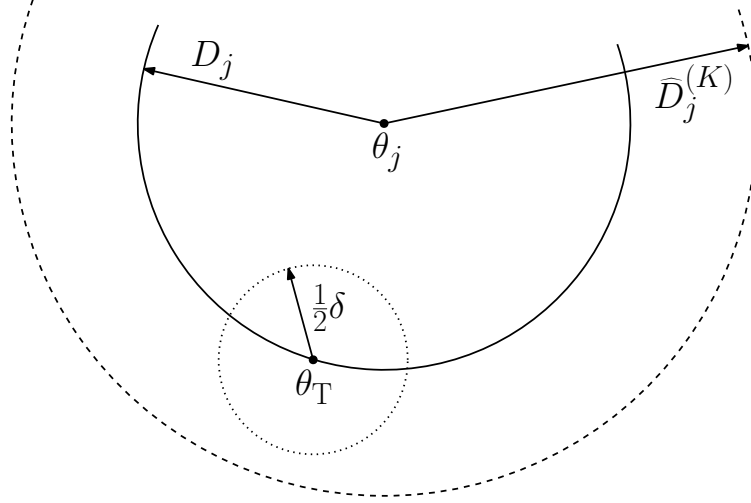


Fig. 8: Geometric illustration of (44).

which yields

$$\mathbb{P}_0(\varpi_j(\delta) = 1) \leq \mathbb{P}_0\left(\mathcal{C}\left(\boldsymbol{\theta}_j, \widehat{D}_j^{(K)}\right) \cap \mathcal{B}\left(\boldsymbol{\theta}_T, \frac{1}{2}\delta\right) = \emptyset\right) + \mathbb{P}_0(\mathcal{E}_1^C) + \mathbb{P}_0(\mathcal{E}_2^C). \quad (43)$$

In addition, as illustrated in Fig. 8, if $j \in \mathcal{U}$, we know $\boldsymbol{\theta}_T \in \mathcal{C}(\boldsymbol{\theta}_j, D_j)$ which yields that under hypothesis \mathcal{H}_0 ,

$$\left\{\mathcal{C}\left(\boldsymbol{\theta}_j, \widehat{D}_j^{(K)}\right) \cap \mathcal{B}\left(\boldsymbol{\theta}_T, \frac{1}{2}\delta\right) = \emptyset\right\} \Leftrightarrow \left\{\left|\widehat{D}_j^{(K)} - D_j\right| \geq \frac{1}{2}\delta\right\}, \quad (44)$$

and therefore, by employing (37) and (43), the false alarm probability can be bounded from above as per

$$\begin{aligned} \mathbb{P}_0(\varpi_j(\delta) = 1) &\leq \mathbb{P}_0\left(\left|\widehat{D}_j^{(K)} - D_j\right| \geq \frac{1}{2}\delta\right) + \mathbb{P}_0(\mathcal{E}_1^C) + \mathbb{P}_0(\mathcal{E}_2^C) \\ &= \mathbb{P}_0\left(\left|\widehat{D}_j^{(K)} - D_j\right| \geq \frac{1}{2}\delta\right) + \sum_{i=1}^2 \mathbb{P}_0\left(\left|\widehat{D}_{N+i}^{(K)} - D_{N+i}\right| \geq \frac{1}{2}\delta\right). \end{aligned} \quad (45)$$

B. Upper Bound on Miss Probability

On the other hand, the miss probability of the detector in (33) can be bounded from above as per

$$\begin{aligned}
\mathbb{P}_1(\varpi_j(\delta) = 0) &= \mathbb{P}_1\left(\mathcal{C}\left(\boldsymbol{\theta}_j, \widehat{D}_j^{(K)}\right) \cap \left[\bigcap_{i=1}^2 \mathcal{R}\left(\boldsymbol{\theta}_{N+i}, \widehat{D}_{N+i}^{(K)}, \delta\right)\right] \neq \emptyset\right) \\
&= \mathbb{P}_1\left(\left\{\mathcal{C}\left(\boldsymbol{\theta}_j, \widehat{D}_j^{(K)}\right) \cap \left[\bigcap_{i=1}^2 \mathcal{R}\left(\boldsymbol{\theta}_{N+i}, \widehat{D}_{N+i}^{(K)}, \delta\right)\right] \neq \emptyset\right\} \cap (\mathcal{E}_1 \cap \mathcal{E}_2)\right) \\
&\quad + \mathbb{P}_1\left(\left\{\mathcal{C}\left(\boldsymbol{\theta}_j, \widehat{D}_j^{(K)}\right) \cap \left[\bigcap_{i=1}^2 \mathcal{R}\left(\boldsymbol{\theta}_{N+i}, \widehat{D}_{N+i}^{(K)}, \delta\right)\right] \neq \emptyset\right\} \cap (\mathcal{E}_1^C \cup \mathcal{E}_2^C)\right) \\
&\leq \mathbb{P}_1\left(\left\{\mathcal{C}\left(\boldsymbol{\theta}_j, \widehat{D}_j^{(K)}\right) \cap \left[\bigcap_{i=1}^2 \mathcal{R}\left(\boldsymbol{\theta}_{N+i}, D_{N+i}, \frac{3}{2}\delta\right)\right] \neq \emptyset\right\} \cap (\mathcal{E}_1 \cap \mathcal{E}_2)\right) \\
&\quad + \mathbb{P}_1(\mathcal{E}_1^C \cup \mathcal{E}_2^C) \tag{46}
\end{aligned}$$

$$\begin{aligned}
&\leq \mathbb{P}_1\left(\mathcal{C}\left(\boldsymbol{\theta}_j, \widehat{D}_j^{(K)}\right) \cap \left[\bigcap_{i=1}^2 \mathcal{R}\left(\boldsymbol{\theta}_{N+i}, D_{N+i}, \frac{3}{2}\delta\right)\right] \neq \emptyset\right) + \mathbb{P}_1(\mathcal{E}_1^C) + \mathbb{P}_1(\mathcal{E}_2^C) \\
&\leq \mathbb{P}_1\left(\mathcal{C}\left(\boldsymbol{\theta}_j, \widehat{D}_j^{(K)}\right) \cap \mathcal{B}\left(\boldsymbol{\theta}_T, \Phi\left(\frac{3}{2}\delta\right)\right) \neq \emptyset\right) + \mathbb{P}_1(\mathcal{E}_1^C) + \mathbb{P}_1(\mathcal{E}_2^C), \tag{47}
\end{aligned}$$

where (46) is due to the fact that if \mathcal{E}_1 and \mathcal{E}_2 occur, then

$$\mathcal{R}\left(\boldsymbol{\theta}_{N+i}, \widehat{D}_{N+i}^{(K)}, \delta\right) \subseteq \mathcal{R}\left(\boldsymbol{\theta}_{N+i}, D_{N+i}, \frac{3}{2}\delta\right), \quad i = 1, 2, \tag{48}$$

and (47) is because $\bigcap_{i=1}^2 \mathcal{R}\left(\boldsymbol{\theta}_{N+i}, D_{N+i}, \frac{3}{2}\delta\right) \subseteq \mathcal{B}\left(\boldsymbol{\theta}_T, \Phi\left(\frac{3}{2}\delta\right)\right)$ according to Lemma 1.

Since the first term in (47) is hard to deal with, we employ an upper bound on it which is provided in the following lemma.

Lemma 2: Define

$$\lambda_j \triangleq \frac{\kappa D_0 P_0^{\frac{1}{\gamma}} \left[\tau_j - F_j^{-1}\left(\rho_j^{(L)}\right)\right]^{-\frac{\gamma+1}{\gamma}}}{\sup_{x \in [F_j^{-1}(\rho_j^{(L)}), F_j^{-1}(\rho_j^{(U)})]} f_j(x)}, \tag{49}$$

and denote

$$\lambda = \min_{j=1,2,\dots,N} \{\lambda_j\}. \tag{50}$$

If

$$0 < \delta < \min \left\{ \Upsilon, \left\{ (2D_U + \Upsilon)^{\frac{1}{2}} \left[\frac{6D_U + 3\Upsilon}{2D_S} \left(\frac{\Upsilon}{D_S} + 1 \right) + 3 \right]^{\frac{1}{2}} + \frac{1}{2} \Upsilon^{\frac{1}{2}} \right\}^{-2} \lambda^2 \right\}, \tag{51}$$

then

$$\mathbb{P}_1\left(\mathcal{C}\left(\boldsymbol{\theta}_j, \widehat{D}_j^{(K)}\right) \cap \mathcal{B}\left(\boldsymbol{\theta}_T, \Phi\left(\frac{3}{2}\delta\right)\right) \neq \emptyset\right) \leq \mathbb{P}_1\left(\left|\widehat{D}_j^{(K)} - \widetilde{D}_j\right| \geq \frac{1}{2}\delta\right), \tag{52}$$

where \widetilde{D}_j is defined in (27).

Proof: Refer to Appendix B. ■

It is worth mentioning that since $f_j(x)$ is continuous and positive over $\{x|F_j(x) \in (0,1)\}$, the denominator $\sup_{x \in [F_j^{-1}(\rho_j^{(L)}), F_j^{-1}(\rho_j^{(U)})]} f_j(x)$ in (49) is positive and bounded. Moreover, according to (10), we know that $\tau_j > F_j^{-1}(\rho_j^{(L)})$, since F_j^{-1} is strictly increasing. Therefore, $0 < \lambda_j < \infty$, and hence, $0 < \lambda < \infty$.

By employing (47) and Lemma 2, we know if (51) holds, then an upper bound on the miss probability of the detector in (33) can be expressed as

$$\begin{aligned} \mathbb{P}_1(\varpi_j(\delta) = 0) &\leq \mathbb{P}_1\left(\left|\widehat{D}_j^{(K)} - \widetilde{D}_j\right| \geq \frac{1}{2}\delta\right) + \mathbb{P}_1(\mathcal{E}_1^C) + \mathbb{P}_1(\mathcal{E}_2^C) \\ &= \mathbb{P}_1\left(\left|\widehat{D}_j^{(K)} - \widetilde{D}_j\right| \geq \frac{1}{2}\delta\right) + \sum_{i=1}^2 \mathbb{P}_1\left(\left|\widehat{D}_{N+i}^{(K)} - D_{N+i}\right| \geq \frac{1}{2}\delta\right). \end{aligned} \quad (53)$$

C. Exponential Decay of False Alarm and Miss Probabilities

It is seen from (45) and (53) that the upper bounds on the false alarm and miss probabilities have some similarities. To be specific, since the $(N+1)$ -th and $(N+2)$ -th sensors are secure, $\mathbb{P}_0\left(\left|\widehat{D}_{N+i}^{(K)} - D_{N+i}\right| \geq \frac{1}{2}\delta\right) = \mathbb{P}_1\left(\left|\widehat{D}_{N+i}^{(K)} - D_{N+i}\right| \geq \frac{1}{2}\delta\right)$ for $i = 1, 2$. Thus, the second term in (45) is the same as the second term in (53). Moreover, as $K \rightarrow \infty$, $\widehat{D}_j^{(K)} \rightarrow D_j$ almost surely under hypothesis \mathcal{H}_0 , while $\widehat{D}_j^{(K)} \rightarrow \widetilde{D}_j$ almost surely under hypothesis \mathcal{H}_1 , one can expect that the first term in (45) and the first term in (53) behave in a very similar way as K increases, except for the change in $\widehat{D}_j^{(K)}$ due to the attack. In the following theorem, by employing (45) and (53), we show that the false alarm and miss probabilities of the detector in (33) decay at least exponentially with respect to K .

Theorem 1: If (51) holds, then the false alarm and miss probabilities are upper bounded by

$$\mathbb{P}_0(\varpi_j(\delta) = 1) \leq 12e^{-\eta_j^{(0)}(\delta)K}, \quad (54)$$

$$\mathbb{P}_1(\varpi_j(\delta) = 0) \leq 12e^{-\eta_j^{(1)}(\delta)K}, \quad (55)$$

for some positive constants $\eta_j^{(0)}(\delta)$ and $\eta_j^{(1)}(\delta)$.

Proof: Before proceeding, we define a sequence of events $\mathcal{F}_{j,K}$ as

$$\mathcal{F}_{j,K} \triangleq \left\{ \xi_j^{(K)} \in \left[\varepsilon_j^{(L)}, \varepsilon_j^{(U)} \right] \right\}, \quad (56)$$

where $\xi_j^{(K)}$ is defined in (26). The constants $\varepsilon_j^{(L)}$ and $\varepsilon_j^{(U)}$ in (56) are defined as

$$\varepsilon_j^{(L)} \triangleq \sigma_j^{(L)} \rho_j^{(L)} \quad \text{and} \quad \varepsilon_j^{(U)} \triangleq \sigma_j^{(U)} \rho_j^{(U)} + \left(1 - \sigma_j^{(U)}\right) F_j(\tau_j) \quad (57)$$

for some numbers $\sigma_j^{(L)}, \sigma_j^{(U)} \in (0, 1)$, where $F_j(\tau_j) \triangleq \int_{-\infty}^{\tau_j} f_j(t) dt$, and $\rho_j^{(L)}$ and $\rho_j^{(U)}$ are defined in (10) and (11), respectively. From (16) and (57), we know that

$$0 < \varepsilon_j^{(L)} < \rho_j^{(L)} < \rho_j^{(U)} < \varepsilon_j^{(U)} < F_j(\tau_j) \leq 1. \quad (58)$$

Let's first consider the upper bound on the false alarm probability as illustrated in (45). For any $j \in \{1, 2, \dots, N + 2\}$,

$$\begin{aligned} \mathbb{P}_0 \left(\left| \widehat{D}_j^{(K)} - D_j \right| \geq \frac{1}{2} \delta \right) &= \mathbb{P}_0 \left(\left\{ \left| \widehat{D}_j^{(K)} - D_j \right| \geq \frac{1}{2} \delta \right\} \cap \mathcal{F}_{j,K} \right) \\ &\quad + \mathbb{P}_0 \left(\left\{ \left| \widehat{D}_j^{(K)} - D_j \right| \geq \frac{1}{2} \delta \right\} \cap \mathcal{F}_{j,K}^C \right) \\ &\leq \mathbb{P}_0 \left(\left\{ \left| \widehat{D}_j^{(K)} - D_j \right| \geq \frac{1}{2} \delta \right\} \cap \mathcal{F}_{j,K} \right) + \mathbb{P}_0(\mathcal{F}_{j,K}^C). \end{aligned} \quad (59)$$

Note that under hypothesis \mathcal{H}_0 , if $\xi_j^{(K)} \in [\varepsilon_j^{(L)}, \varepsilon_j^{(U)}]$, then by employing (24), (25) and (58), we can obtain

$$\begin{aligned} \left| \widehat{D}_j^{(K)} - D_j \right| &= D_0 P_0^{\frac{1}{\gamma}} \left| \left[\tau_j - F_j^{-1}(\xi_j^{(K)}) \right]^{-\frac{1}{\gamma}} - \left[\tau_j - F_j^{-1}(p_j(\boldsymbol{\theta}_T)) \right]^{-\frac{1}{\gamma}} \right| \\ &\leq D_0 P_0^{\frac{1}{\gamma}} \sup_{x \in [\varepsilon_j^{(L)}, \varepsilon_j^{(U)}]} \left| \frac{\partial \left[\tau_j - F_j^{-1}(x) \right]^{-\frac{1}{\gamma}}}{\partial x} \right| \left| \xi_j^{(K)} - p_j(\boldsymbol{\theta}_T) \right| \\ &= D_0 P_0^{\frac{1}{\gamma}} \sup_{x \in [\varepsilon_j^{(L)}, \varepsilon_j^{(U)}]} \left| \frac{\left[\tau_j - F_j^{-1}(x) \right]^{-\frac{\gamma+1}{\gamma}}}{f_j(F_j^{-1}(x))} \right| \left| \xi_j^{(K)} - p_j(\boldsymbol{\theta}_T) \right| \\ &\leq \underbrace{\frac{D_0 P_0^{\frac{1}{\gamma}} \left[\tau_j - F_j^{-1}(\varepsilon_j^{(U)}) \right]^{-\frac{\gamma+1}{\gamma}}}{\inf_{x \in [F_j^{-1}(\varepsilon_j^{(L)}), F_j^{-1}(\varepsilon_j^{(U)})]} f_j(x)}}_{\Xi_j} \left| \xi_j^{(K)} - p_j(\boldsymbol{\theta}_T) \right|, \end{aligned} \quad (60)$$

where (60) is due to the fact that $p_j(\boldsymbol{\theta}_T) \in [\varepsilon_j^{(L)}, \varepsilon_j^{(U)}]$ and $\xi_j^{(K)} \in [\varepsilon_j^{(L)}, \varepsilon_j^{(U)}]$. Since $f_j(x)$ is continuous and $0 < f_j(x) < \infty$ over $\{x | F_j(x) \in (0, 1)\}$, we know

$$\inf_{x \in [F_j^{-1}(\varepsilon_j^{(L)}), F_j^{-1}(\varepsilon_j^{(U)})]} f_j(x) = \min_{x \in [F_j^{-1}(\varepsilon_j^{(L)}), F_j^{-1}(\varepsilon_j^{(U)})]} f_j(x) \in (0, \infty), \quad (62)$$

and moreover, from (58), we know

$$\tau_j - F_j^{-1}(\varepsilon_j^{(U)}) > 0, \quad (63)$$

since $\varepsilon_j^{(U)} < F_j(\tau_j)$. Therefore, it is clear that $\Xi_j \in (0, \infty)$.

By employing (61), we can obtain

$$\begin{aligned}
& \mathbb{P}_0 \left(\left\{ \left| D_j^{(K)} - D_j \right| \geq \frac{1}{2} \delta \right\} \cap \mathcal{F}_{j,K} \right) \\
& \leq \mathbb{P}_0 \left(\left\{ \Xi_j \left| \xi_j^{(K)} - p_j(\boldsymbol{\theta}_T) \right| \geq \frac{1}{2} \delta \right\} \cap \mathcal{F}_{j,K} \right) \\
& \leq \mathbb{P}_0 \left(\xi_j^{(K)} - p_j(\boldsymbol{\theta}_T) \geq \frac{\delta}{2\Xi_j} \right) + \mathbb{P}_0 \left(\xi_j^{(K)} - p_j(\boldsymbol{\theta}_T) \leq -\frac{\delta}{2\Xi_j} \right) \\
& = \mathbb{P}_0 \left(\underbrace{\sum_{k=1}^K (1 - \tilde{u}_{jk} - p_j(\boldsymbol{\theta}_T))}_{X_{jk}} \geq \frac{\delta}{2\Xi_j} K \right) + \mathbb{P}_0 \left(\underbrace{\sum_{k=1}^K (\tilde{u}_{jk} + p_j(\boldsymbol{\theta}_T) - 1)}_{Y_{jk}} \geq \frac{\delta}{2\Xi_j} K \right). \quad (64)
\end{aligned}$$

It is easy to see that under hypothesis \mathcal{H}_0 , $\{X_{jk}\}_{k=1}^K$ is a sequence of independent and identically distributed random variables with distribution

$$q_{X_j} \triangleq \mathbb{P}_0(X_{jk} = 1 - p_j(\boldsymbol{\theta}_T)) = p_j(\boldsymbol{\theta}_T) \quad (65)$$

$$\bar{q}_{X_j} \triangleq \mathbb{P}_0(X_{jk} = -p_j(\boldsymbol{\theta}_T)) = 1 - p_j(\boldsymbol{\theta}_T). \quad (66)$$

Since

$$\frac{\delta}{2\Xi_j} K > \mathbb{E}_0\{X_{jk}\} = [1 - p_j(\boldsymbol{\theta}_T)] q_{X_j} - p_j(\boldsymbol{\theta}_T) \bar{q}_{X_j} = 0, \quad (67)$$

by employing the large deviations theory [20], we can obtain

$$\mathbb{P}_0 \left(\sum_{k=1}^K (1 - \tilde{u}_{jk} - p_j(\boldsymbol{\theta}_T)) \geq \frac{\delta}{2\Xi_j} K \right) \leq e^{-\eta_{j,1}(\delta)K}, \quad (68)$$

where the rate function $\eta_{j,1}(\delta)$ is defined as

$$\begin{aligned}
\eta_{j,1}(\delta) & \triangleq - \lim_{K \rightarrow \infty} \frac{1}{K} \ln \mathbb{P}_0 \left(\sum_{k=1}^K X_{jk} \geq \frac{\delta}{2\Xi_j} K \right) \\
& = \frac{\delta}{2\Xi_j} \mu^* - \ln \phi_{X_j}(\mu^*), \quad (69)
\end{aligned}$$

$$\text{and } \phi_{X_j}(\mu) \triangleq \mathbb{E}_0 \{ e^{\mu X_{jk}} \} = p_j(\boldsymbol{\theta}_T) e^{\mu(1-p_j(\boldsymbol{\theta}_T))} + (1 - p_j(\boldsymbol{\theta}_T)) e^{-\mu p_j(\boldsymbol{\theta}_T)}. \quad (70)$$

Moreover, the quantity μ^* in (69) is the solution of the equation

$$\frac{d}{d\mu} \phi_{X_j}(\mu) = \frac{\delta}{2\Xi_j} \phi_{X_j}(\mu). \quad (71)$$

By employing (69)–(71), the rate function $\eta_{j,1}(\delta)$ can be obtained as

$$\eta_{j,1}(\delta) = \eta_{j,1}^*(\delta) \triangleq \left(\frac{\delta}{2\Xi_j} + p_j(\boldsymbol{\theta}_T) \right) \ln \frac{\left(\frac{\delta}{2\Xi_j} + p_j(\boldsymbol{\theta}_T) \right) (1 - p_j(\boldsymbol{\theta}_T))}{p_j(\boldsymbol{\theta}_T) \left(1 - \frac{\delta}{2\Xi_j} - p_j(\boldsymbol{\theta}_T) \right)} - \ln \frac{1 - p_j(\boldsymbol{\theta}_T)}{1 - \frac{\delta}{2\Xi_j} - p_j(\boldsymbol{\theta}_T)}, \quad (72)$$

provided that

$$\frac{\delta}{2\Xi_j} \leq 1 - p_j(\boldsymbol{\theta}_T). \quad (73)$$

It is seen from (65) and (66) that

$$\sum_{k=1}^K (1 - \tilde{u}_{jk} - p_j(\boldsymbol{\theta}_T)) \leq (1 - p_j(\boldsymbol{\theta}_T)) K, \quad (74)$$

which implies that for the case where $\frac{\delta}{2\Xi_j} > 1 - p_j(\boldsymbol{\theta}_T)$,

$$\mathbb{P}_0 \left(\sum_{k=1}^K (1 - \tilde{u}_{jk} - p_j(\boldsymbol{\theta}_T)) \geq \frac{\delta}{2\Xi_j} K \right) = 0. \quad (75)$$

Therefore, the rate function $\eta_{j,1}(\delta)$ can be written as¹

$$\eta_{j,1}(\delta) = \eta_{j,1}^*(\delta) \mathbb{1} \left\{ \frac{\delta}{2\Xi_j} \leq 1 - p_j(\boldsymbol{\theta}_T) \right\} + \infty \mathbb{1} \left\{ \frac{\delta}{2\Xi_j} > 1 - p_j(\boldsymbol{\theta}_T) \right\}, \quad (76)$$

where $\eta_{j,1}^*(\delta)$ is defined in (72).

Similarly, noting that under hypothesis \mathcal{H}_0 , $\{Y_{jk}\}_{k=1}^K$ is a sequence of independent and identically distributed random variables with distribution

$$q_{X_j} \triangleq \mathbb{P}_0(Y_{jk} = p_j(\boldsymbol{\theta}_T) - 1) = p_j(\boldsymbol{\theta}_T) \quad (77)$$

$$\bar{q}_{X_j} \triangleq \mathbb{P}_0(Y_{jk} = p_j(\boldsymbol{\theta}_T)) = 1 - p_j(\boldsymbol{\theta}_T), \quad (78)$$

we can obtain

$$\mathbb{P}_0 \left(\sum_{k=1}^K (\tilde{u}_{jk} + p_j(\boldsymbol{\theta}_T) - 1) \geq \frac{\delta}{2\Xi_j} K \right) \leq e^{-\eta_{j,2}(\delta)K}, \quad (79)$$

where the rate function $\eta_{j,2}(\delta)$ is given by

$$\eta_{j,2}(\delta) = \eta_{j,2}^*(\delta) \mathbb{1} \left\{ \frac{\delta}{2\Xi_j} \leq p_j(\boldsymbol{\theta}_T) \right\} + \infty \mathbb{1} \left\{ \frac{\delta}{2\Xi_j} > p_j(\boldsymbol{\theta}_T) \right\} \quad (80)$$

$$\text{with } \eta_{j,2}^*(\delta) \triangleq \ln \frac{1 + \frac{\delta}{2\Xi_j} - p_j(\boldsymbol{\theta}_T)}{1 - p_j(\boldsymbol{\theta}_T)} - \left(p_j(\boldsymbol{\theta}_T) - \frac{\delta}{2\Xi_j} \right) \ln \frac{p_j(\boldsymbol{\theta}_T) \left(1 + \frac{\delta}{2\Xi_j} - p_j(\boldsymbol{\theta}_T) \right)}{\left(p_j(\boldsymbol{\theta}_T) - \frac{\delta}{2\Xi_j} \right) (1 - p_j(\boldsymbol{\theta}_T))}. \quad (81)$$

As a result, from (64), (68) and (79), we can obtain

$$\mathbb{P}_0 \left(\left\{ \left| D_j^{(K)} - D_j \right| \geq \frac{1}{2} \delta \right\} \cap \mathcal{F}_{j,K} \right) \leq e^{-\eta_{j,1}(\delta)K} + e^{-\eta_{j,2}(\delta)K}, \quad (82)$$

where $\eta_{j,1}(\delta)$ and $\eta_{j,2}(\delta)$ are defined in (76) and (80), respectively.

¹Regarding the second term of the right-hand side of (76), we define $\infty \cdot 0 = 0$.

Now, we consider the second term in (59). From (12) and (58), we know

$$0 < \varepsilon_j^{(L)} < p_j(\boldsymbol{\theta}_T) < \varepsilon_j^{(U)} < 1, \quad (83)$$

and hence, by employing similar arguments, we can obtain

$$\begin{aligned} \mathbb{P}_0(\mathcal{F}_{j,K}^C) &= \mathbb{P}_0\left(\xi_j^{(K)} \notin [\varepsilon_j^{(L)}, \varepsilon_j^{(U)}]\right) \\ &= \mathbb{P}_0\left(\xi_j^{(K)} > \varepsilon_j^{(U)}\right) + \mathbb{P}_0\left(\xi_j^{(K)} < \varepsilon_j^{(L)}\right) \\ &\leq \mathbb{P}_0\left(\sum_{k=1}^K 1 - \tilde{u}_{jk} - p_j(\boldsymbol{\theta}_T) \geq (\varepsilon_j^{(U)} - p_j(\boldsymbol{\theta}_T))K\right) \\ &\quad + \mathbb{P}_0\left(\sum_{k=1}^K \tilde{u}_{jk} + p_j(\boldsymbol{\theta}_T) - 1 \geq (p_j(\boldsymbol{\theta}_T) - \varepsilon_j^{(L)})K\right) \\ &\leq e^{-\eta_{\varepsilon_j^{(U)}}K} + e^{-\eta_{\varepsilon_j^{(L)}}K}, \end{aligned} \quad (84)$$

where the rate functions can be expressed as

$$\eta_{\varepsilon_j^{(U)}} = \varepsilon_j^{(U)} \ln \frac{\varepsilon_j^{(U)} (1 - p_j(\boldsymbol{\theta}_T))}{p_j(\boldsymbol{\theta}_T) (1 - \varepsilon_j^{(U)})} - \ln \frac{1 - p_j(\boldsymbol{\theta}_T)}{1 - \varepsilon_j^{(U)}}, \quad (85)$$

$$\text{and } \eta_{\varepsilon_j^{(L)}} = \ln \frac{1 - \varepsilon_j^{(L)}}{1 - p_j(\boldsymbol{\theta}_T)} - \varepsilon_j^{(L)} \ln \frac{p_j(\boldsymbol{\theta}_T) (1 - \varepsilon_j^{(L)})}{\varepsilon_j^{(L)} (1 - p_j(\boldsymbol{\theta}_T))}. \quad (86)$$

It is worth noticing that $\eta_{\varepsilon_j^{(L)}}$ and $\eta_{\varepsilon_j^{(U)}}$ do not depend on δ .

As a result, from (59), (82) and (84), we know that for any $j \in \{1, 2, \dots, N+2\}$, $\mathbb{P}_0(|\widehat{D}_j^{(K)} - D_j| \geq \frac{1}{2}\delta)$ can be bounded from above as per

$$\mathbb{P}_0\left(|\widehat{D}_j^{(K)} - D_j| \geq \frac{1}{2}\delta\right) \leq e^{-\eta_{j,1}(\delta)K} + e^{-\eta_{j,2}(\delta)K} + e^{-\eta_{\varepsilon_j^{(L)}}K} + e^{-\eta_{\varepsilon_j^{(U)}}K}, \quad (87)$$

which yields an upper bound on the false alarm probability of the detector in (33)

$$\begin{aligned} \mathbb{P}_0(\varpi_j(\delta) = 1) &\leq \sum_{i=j, N+1, N+2} e^{-\eta_{i,1}(\delta)K} + e^{-\eta_{i,2}(\delta)K} + e^{-\eta_{\varepsilon_i^{(U)}}K} + e^{-\eta_{\varepsilon_i^{(L)}}K} \\ &\leq 12e^{-\eta_j^{(0)}(\delta)K}, \end{aligned} \quad (88)$$

$$\text{with } \eta_j^{(0)}(\delta) \triangleq \min_{i=j, N+1, N+2} \left\{ \eta_{i,1}(\delta), \eta_{i,2}(\delta), \eta_{\varepsilon_i^{(L)}}, \eta_{\varepsilon_i^{(U)}} \right\}. \quad (89)$$

Next, we consider the upper bound on the miss detection probability as given in (53).

By employing (18) and following the steps for obtaining (76), (80), (85), (86) and (87), we can obtain

$$\mathbb{P}_1\left(\left|D_j^{(K)} - \widetilde{D}_j\right| \geq \frac{1}{2}\delta\right) \leq e^{-\tilde{\eta}_{j,1}(\delta)K} + e^{-\tilde{\eta}_{j,2}(\delta)K} + e^{-\tilde{\eta}_{\varepsilon_j^{(L)}}K} + e^{-\tilde{\eta}_{\varepsilon_j^{(U)}}K} \quad (90)$$

where $\tilde{\eta}_{j,1}(\delta)$, $\tilde{\eta}_{j,2}(\delta)$, $\tilde{\eta}_{\varepsilon_j^{(L)}}$ and $\tilde{\eta}_{\varepsilon_j^{(U)}}$ can be expressed as

$$\tilde{\eta}_{j,1}(\delta) = \tilde{\eta}_{j,1}^*(\delta) \mathbb{1} \left\{ \frac{\delta}{2\Xi_j} \leq 1 - \tilde{p}_j(\boldsymbol{\theta}_T) \right\} + \infty \mathbb{1} \left\{ \frac{\delta}{2\Xi_j} > 1 - \tilde{p}_j(\boldsymbol{\theta}_T) \right\}, \quad (91)$$

$$\tilde{\eta}_{j,2}(\delta) = \tilde{\eta}_{j,2}^*(\delta) \mathbb{1} \left\{ \frac{\delta}{2\Xi_j} \leq \tilde{p}_j(\boldsymbol{\theta}_T) \right\} + \infty \mathbb{1} \left\{ \frac{\delta}{2\Xi_j} > \tilde{p}_j(\boldsymbol{\theta}_T) \right\}, \quad (92)$$

$$\tilde{\eta}_{\varepsilon_j^{(L)}} = \ln \frac{1 - \varepsilon_j^{(L)}}{1 - \tilde{p}_j(\boldsymbol{\theta}_T)} - \varepsilon_j^{(L)} \ln \frac{\tilde{p}_j(\boldsymbol{\theta}_T) (1 - \varepsilon_j^{(L)})}{\varepsilon_j^{(L)} (1 - \tilde{p}_j(\boldsymbol{\theta}_T))}. \quad (93)$$

$$\tilde{\eta}_{\varepsilon_j^{(U)}} = \varepsilon_j^{(U)} \ln \frac{\varepsilon_j^{(U)} (1 - \tilde{p}_j(\boldsymbol{\theta}_T))}{\tilde{p}_j(\boldsymbol{\theta}_T) (1 - \varepsilon_j^{(U)})} - \ln \frac{1 - \tilde{p}_j(\boldsymbol{\theta}_T)}{1 - \varepsilon_j^{(U)}}, \quad (94)$$

and $\tilde{\eta}_{j,1}^*(\delta)$ and $\tilde{\eta}_{j,2}^*(\delta)$ are defined as

$$\tilde{\eta}_{j,1}^*(\delta) \triangleq \left(\frac{\delta}{2\Xi_j} + \tilde{p}_j(\boldsymbol{\theta}_T) \right) \ln \frac{\left(\frac{\delta}{2\Xi_j} + \tilde{p}_j(\boldsymbol{\theta}_T) \right) (1 - \tilde{p}_j(\boldsymbol{\theta}_T))}{\tilde{p}_j(\boldsymbol{\theta}_T) \left(1 - \frac{\delta}{2\Xi_j} - \tilde{p}_j(\boldsymbol{\theta}_T) \right)} - \ln \frac{1 - \tilde{p}_j(\boldsymbol{\theta}_T)}{1 - \frac{\delta}{2\Xi_j} - \tilde{p}_j(\boldsymbol{\theta}_T)}, \quad (95)$$

$$\tilde{\eta}_{j,2}^*(\delta) \triangleq \ln \frac{1 + \frac{\delta}{2\Xi_j} - \tilde{p}_j(\boldsymbol{\theta}_T)}{1 - \tilde{p}_j(\boldsymbol{\theta}_T)} - \left(\tilde{p}_j(\boldsymbol{\theta}_T) - \frac{\delta}{2\Xi_j} \right) \ln \frac{\tilde{p}_j(\boldsymbol{\theta}_T) \left(1 + \frac{\delta}{2\Xi_j} - \tilde{p}_j(\boldsymbol{\theta}_T) \right)}{\left(\tilde{p}_j(\boldsymbol{\theta}_T) - \frac{\delta}{2\Xi_j} \right) (1 - \tilde{p}_j(\boldsymbol{\theta}_T))}. \quad (96)$$

Moreover, noticing that

$$\mathbb{P}_1 \left(\left| \hat{D}_{N+i}^{(K)} - D_{N+i} \right| \geq \frac{1}{2} \delta \right) = \mathbb{P}_0 \left(\left| \hat{D}_{N+i}^{(K)} - D_{N+i} \right| \geq \frac{1}{2} \delta \right), \quad i = 1, 2, \quad (97)$$

by employing (53), (87) and (90), we can obtain

$$\begin{aligned} \mathbb{P}_1(\varpi_j(\delta) = 0) &\leq e^{-\tilde{\eta}_{j,1}(\delta)K} + e^{-\tilde{\eta}_{j,2}(\delta)K} + e^{-\tilde{\eta}_{\varepsilon_j^{(L)}}K} + e^{-\tilde{\eta}_{\varepsilon_j^{(U)}}K} \\ &\quad + \sum_{i=N+1}^{N+2} e^{-\eta_{i,1}(\delta)K} + e^{-\eta_{i,2}(\delta)K} + e^{-\eta_{\varepsilon_i^{(U)}}K} + e^{-\eta_{\varepsilon_i^{(L)}}K} \\ &\leq 12e^{-\eta_j^{(1)}(\delta)K}, \end{aligned} \quad (98)$$

where the quantity $\eta_j^{(1)}(\delta)$ is defined as

$$\eta_j^{(1)}(\delta) \triangleq \min_{i=N+1, N+2} \left\{ \tilde{\eta}_{j,1}(\delta), \tilde{\eta}_{j,2}(\delta), \eta_{i,1}(\delta), \tilde{\eta}_{\varepsilon_j^{(L)}}, \tilde{\eta}_{\varepsilon_j^{(U)}}, \eta_{i,1}(\delta), \eta_{\varepsilon_i^{(L)}}, \eta_{\varepsilon_i^{(U)}} \right\}. \quad (99)$$

■

As demonstrated by Theorem 1, the false alarm and miss probabilities of the proposed detector in (33) are guaranteed to decay exponentially as K increases. The decay rates are illustrated in (89) and (99) which depend on the choice of δ . In general, a smaller δ leads to a larger false alarm probability and

a smaller miss probability. Hence, the trade-off between the false alarm and miss probabilities can be sought via altering the value of δ .

Using Theorem 1, the average detector error probability P_e can be bounded from above as per

$$\begin{aligned} P_e &= \frac{1}{N} \sum_{j \in \mathcal{U}} \mathbb{P}_0(\varpi_j = 1) + \frac{1}{N} \sum_{j \in \mathcal{V}} \mathbb{P}_1(\varpi_j = 0) \\ &\leq \frac{12}{N} \sum_{j \in \mathcal{U}} e^{-\eta_j^{(0)}(\delta)K} + \frac{12}{N} \sum_{j \in \mathcal{V}} e^{-\eta_j^{(1)}(\delta)K} \\ &\leq C_e e^{-\eta_e(\delta)K}, \end{aligned} \quad (100)$$

where the positive constants C_e and $\eta_e(\delta)$ are defined as

$$C_e = 12 \quad \text{and} \quad \eta_e(\delta) \triangleq \min_{j=1,2,\dots,N} \left\{ \eta_j^{(0)}(\delta), \eta_j^{(1)}(\delta) \right\}. \quad (101)$$

This observation is summarized in the following corollary.

Corollary 1: If (51) holds, then the average detector error probability decreases at least exponentially as K increases.

It is worth pointing out that the sufficient condition on δ in Theorem 1 and Corollary 1 are generally not necessary, which is observed in all the numerical experiments that we carried out.

V. SIMULATION RESULTS

In this section, we first introduce how to implement the proposed attack detector in practice, and then we test the performance of the proposed attack detector to corroborate the theoretical results in previous sections.

A. Implementation of the Attack Detector

By employing (25), $\widehat{D}_j^{(K)}$, $\widehat{D}_{N+1}^{(K)}$ and $\widehat{D}_{N+2}^{(K)}$ can be computed, and thereby the analytical expression of $\mathcal{C}(\boldsymbol{\theta}_j, \widehat{D}_j^{(K)})$ can be obtained. Note that every point $\boldsymbol{\theta}$ in the common area of $\mathcal{R} = (\boldsymbol{\theta}_{N+1}, \widehat{D}_{N+1}^{(K)}, \delta)$ and $\mathcal{R}(\boldsymbol{\theta}_{N+2}, \widehat{D}_{N+2}^{(K)}, \delta)$ satisfies the condition

$$\begin{cases} -\delta \leq \|\boldsymbol{\theta} - \boldsymbol{\theta}_{N+1}\| - \widehat{D}_{N+1}^{(K)} \leq \delta, \\ -\delta \leq \|\boldsymbol{\theta} - \boldsymbol{\theta}_{N+2}\| - \widehat{D}_{N+2}^{(K)} \leq \delta. \end{cases} \quad (102)$$

Therefore, to implement the attack detector in (33), we only need to check whether any point on the circle $\mathcal{C}(\boldsymbol{\theta}_j, \widehat{D}_j^{(K)})$ satisfies the condition in (102) or not.

One brute force way to do this is to discretize $\mathcal{C}(\boldsymbol{\theta}_j, \widehat{D}_j^{(K)})$ to finitely many points which are evenly spaced along the circle, and then we check the condition in (102) for these points. In particular, we can discretize $\mathcal{C}(\boldsymbol{\theta}_j, \widehat{D}_j^{(K)})$ to M points $\{\boldsymbol{\theta}_C^{(m)}\}_{m=1}^M$ in the way that

$$\boldsymbol{\theta}_C^{(m)} = \left[x_j + \widehat{D}_j^{(K)} \cos\left(\frac{2\pi}{M}(m-1)\right), y_j + \widehat{D}_j^{(K)} \sin\left(\frac{2\pi}{M}(m-1)\right) \right], \quad (103)$$

where x_j and y_j are the coordinates of the j -th sensor. We summarize this implementation in Algorithm 1. Intuitively, we expect that this approach may not work well for small M .

Algorithm 1 Implementation of attack detector

- 1: **Input:** $\{u_{ik}\}_{k=1}^K$ for $i = N + 1, N + 2$, $\{\tilde{u}_{jk}\}_{k=1}^K$, and δ ;
 - 2: **Output:** $\varpi_j(\delta)$;
 - 3: Compute $\widehat{D}_j^{(K)}$, $\widehat{D}_{N+1}^{(K)}$ and $\widehat{D}_{N+2}^{(K)}$ by employing (25);
 - 4: Discretize $\mathcal{C}(\boldsymbol{\theta}_j, \widehat{D}_j^{(K)})$ to $\{\boldsymbol{\theta}_C^{(m)}\}_{m=1}^M$ by employing (103);
 - 5: $m \leftarrow 1$ **and** $\varpi_j(\delta) \leftarrow 1$;
 - 6: **while** $m \leq M$ **and** $\varpi_j(\delta) = 1$ **do**
 - 7: **if** $\boldsymbol{\theta}_C^{(m)} \in \mathcal{S}$ **and** (102) holds **then**
 - 8: $\varpi_j(\delta) \leftarrow 0$;
 - 9: **end if**
 - 10: $m \leftarrow m + 1$;
 - 11: **end while**
-

B. Simulation Setup and Results

The simulation setup is illustrated in Fig. 9. Consider a sensor network consisting of two groups of sensors with $N = 500$. The two secure sensors are located at $\boldsymbol{\theta}_{501} = (-10^3, 0)$ and $\boldsymbol{\theta}_{502} = (10^3, 0)$, respectively. The rest of sensors are all located along the x -axis, and are partitioned into two groups. The first group of sensors $\{1, 2, \dots, 250, 501\}$ are evenly spaced between $(-10^3, 0)$ and $(-0.9 \times 10^3, 0)$, while the second group of sensors $\{251, 252, \dots, 500, 502\}$ are evenly spaced between $(0.9 \times 10^3, 0)$ and $(10^3, 0)$. The ROI \mathcal{A} is a disc centered at $(0, 10^5)$ and with radius equal to 7500. The target is located at $\boldsymbol{\theta}_T = (0, 10^5)$. In the simulation, $P_0 = 1$, $D_0 = 10^5$, and $\gamma = 2$. When employing Algorithm 1 to implement the attack detector, M is chosen to be 2×10^5 . In addition, the threshold $\tau_j = 1$ for all j , and n_{jk} follows a Gaussian distribution with zero mean and unit variance. We assume that 250

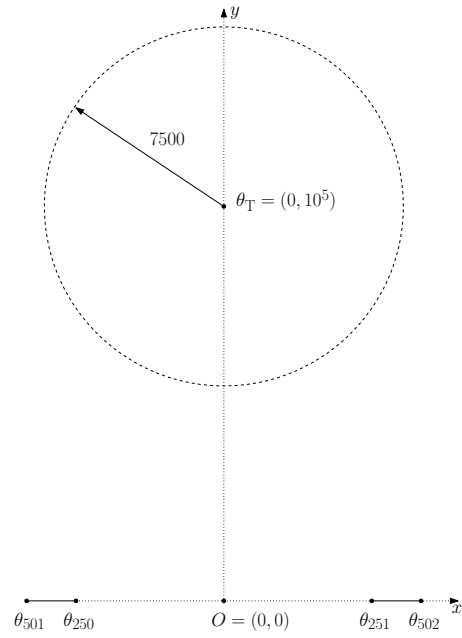


Fig. 9: Simulation setup.

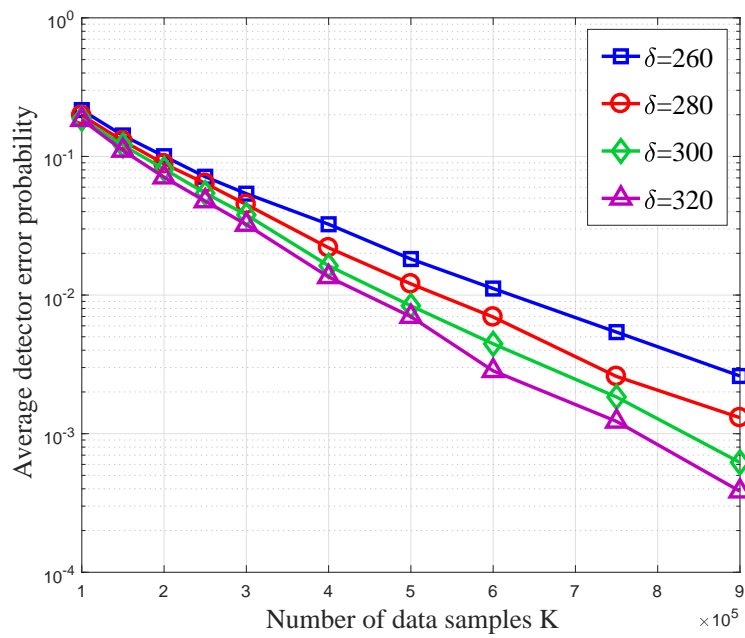


Fig. 10: Attack identification performance of the proposed detectors.

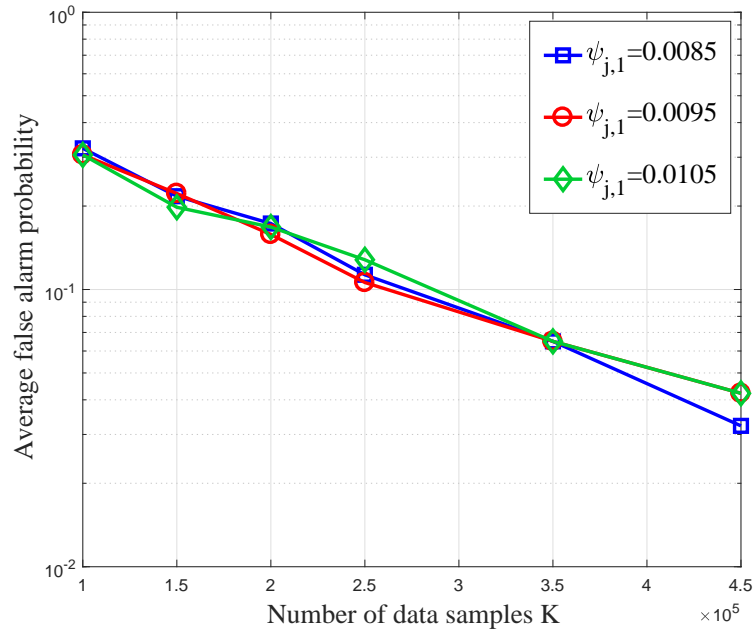


Fig. 11: Average false alarm probabilities of the proposed detector under different attacks.

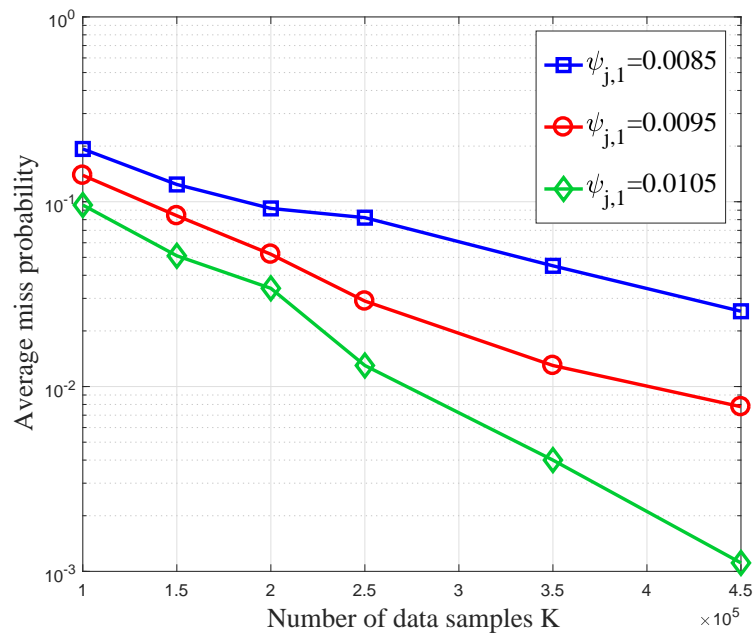


Fig. 12: Average miss probabilities of the proposed detector under different attacks.

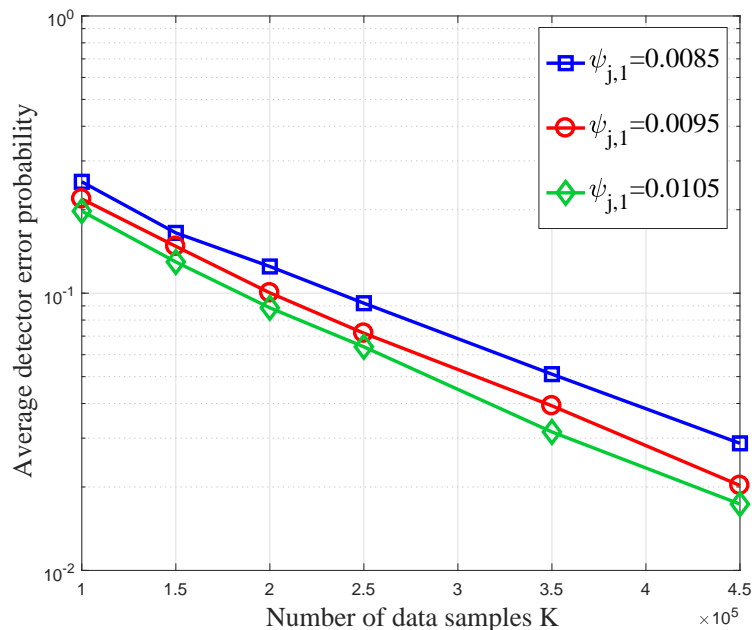


Fig. 13: Attack identification performance of the proposed detector under different attacks.

sensors $\{1, 2, \dots, 250\}$ are under the MiMA as described in (19) with $\psi_{j,0} = 0$ and $\psi_{j,1} = 0.0105$ for $j = 1, 2, \dots, 250$. The average detector error probability over 900 Monte Carlo runs versus the number K of data samples are depicted on a log scale in Fig. 10 for four detectors with $\delta = 260, 280, 300, 320$, respectively. It is seen from Fig. 10 that for each detector, the average detector error probability decreases exponentially as K grows which agrees with the theoretical results in the previous section. Moreover, as illustrated in Fig. 10, the larger the value of δ , the better the identification performance, which implies that in this simulation, as δ increases, the gain obtained in the false alarm probability is larger than the loss in the miss probability, since the number of attacked sensors is the same as the number of unattacked sensors.

Now, we consider the attack identification performance of the proposed detector under different attacks. In Fig. 11, Fig. 12 and Fig. 13, the simulation setup is the same as that for Fig. 10, except $\delta = 280$. The different attacks are all MiMA and for $j = 1, 2, \dots, 250$, $[\psi_{j,0}, \psi_{j,1}] = [0, 0.0085]$, $[0, 0.0095]$, and $[0, 0.0105]$, respectively. It is seen from Fig. 11 that under different attacks, the false alarm probabilities achieved by the detector are very close, which agrees with the fact that the false alarm probability does not depend on the attacks, but is only determined by δ . As expected from the intuition that the attack which brings about a larger impact on the statistical model of the data should be easier to be detected,

Fig. 12 demonstrates that the larger the value of $\psi_{j,1}$, the smaller the average miss probability. Fig. 13 also corroborates the intuition that the larger the attack impact on the statistical model of the data, the better the attack identification performance that can be achieved.

VI. CONCLUSIONS

This work has investigated the attack detection in sensor network target localization systems with quantized data. By exploring the impact of the attacks on the statistical model of the sensor data, we have revealed that from the perspective of the NMLE, the essential effect of attacks is a falsification of the estimated distance between the target and each attacked sensor, and hence, gives rise to a geometric inconsistency among the attacked and unattacked sensors. Motivated by this fact, a class of detectors are proposed to detect the attacks in the sensor network via scrutinizing the existence of the geometric inconsistency. A rigorous detection performance analysis for the proposed detectors has been carried out, showing that the false alarm and miss probabilities decay exponentially as the number of data samples at each sensor grows, which implies that for a sufficiently large number of samples, the proposed detectors can identify the attacked sensors with any required level of accuracy.

APPENDIX A

PROOF OF LEMMA 1

Consider R_{N+1} and R_{N+2} which satisfy

$$|R_i - D_i| \leq \delta < \Upsilon, \quad \text{for } i = N + 1, N + 2, \quad (104)$$

and denote

$$\boldsymbol{\theta}'_T \triangleq \mathcal{C}(\boldsymbol{\theta}_{N+1}, R_{N+1}) \cap \mathcal{C}(\boldsymbol{\theta}_{N+2}, R_{N+2}). \quad (105)$$

From (7) and (104), we know that

$$R_{N+1} + R_{N+2} \geq D_{N+1} + D_{N+2} - 2\delta > \inf_{\boldsymbol{\theta}_T \in \mathcal{A}} \{D_{N+1} + D_{N+2}\} - 2\Upsilon_2 = D_S, \quad (106)$$

and moreover, by employing (6) and (104), we can obtain

$$|R_{N+1} - R_{N+2}| < |D_{N+1} - D_{N+2}| + 2\delta < D_U - D_L + 2\Upsilon \leq D_U - D_L + 2\Upsilon_1 < D_S. \quad (107)$$

Thus, R_{N+1} , R_{N+2} and D_S can be the sides of a triangle, and hence, $\boldsymbol{\theta}'_T$ exists and cannot be on the line passing through $\boldsymbol{\theta}_{N+1}$ and $\boldsymbol{\theta}_{N+2}$, which implies that the angle $\beta \triangleq \angle \boldsymbol{\theta}'_T \boldsymbol{\theta}_{N+1} \boldsymbol{\theta}_{N+2}$ in Fig. 14 satisfies $\beta \in (0, \pi)$.

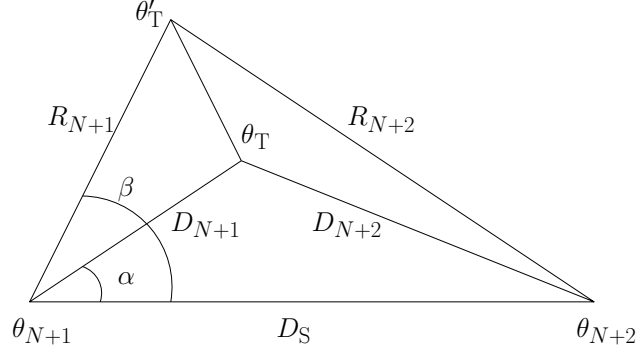


Fig. 14: Geometric illustration.

Let α denote the angle $\angle \theta_T \theta_{N+1} \theta_{N+2}$ as illustrated in Fig. 14. By the law of cosines, we can obtain

$$d(R_{N+1}, R_{N+2}) \triangleq \|\theta'_T - \theta_T\| = R_{N+1}^2 + D_{N+1}^2 - 2R_{N+1}D_{N+1} \cos(\beta - \alpha). \quad (108)$$

According to Assumption 1, we know

$$D_S > |D_{N+1} - D_{N+2}| \quad \text{and} \quad D_{N+1} + D_{N+2} > D_S, \quad (109)$$

which yields $\alpha \in (0, \pi)$, and hence,

$$\beta - \alpha \in (-\pi, \pi). \quad (110)$$

From (108), we know that for any given R_{N+1} , $d(R_{N+1}, R_{N+2})$ is maximized when $\cos(\beta - \alpha)$ is minimized. Since α is fixed and $\beta - \alpha \in (-\pi, \pi)$, $\cos(\beta - \alpha)$ is minimized when β is either maximized or minimized, which implies that $d(R_{N+1}, R_{N+2})$ is maximized when β is either maximized or minimized.

Furthermore, by the law of cosines, we can obtain

$$\cos(\beta) = \frac{R_{N+1}^2 + D_S^2 - R_{N+2}^2}{2R_{N+1}D_S}. \quad (111)$$

Since $\beta \in (0, \pi)$ and $\cos(\beta)$ is decreasing over $\beta \in (0, \pi)$, for any given R_{N+1} , β is maximized if R_{N+2} is maximized, while β is minimized if R_{N+2} is minimized. Therefore, for any given R_{N+1} , $d(R_{N+1}, R_{N+2})$ is maximized only when $R_{N+2} = D_{N+2} + \delta$ or $R_{N+2} = D_{N+2} - \delta$, since $|R_{N+2} - D_{N+2}| \leq \delta$.

Similarly, for any given R_{N+2} , $d(R_{N+1}, R_{N+2})$ is maximized only when $R_{N+1} = D_{N+1} + \delta$ or $R_{N+1} = D_{N+1} - \delta$.

Thus, for any given R_{N+1} and R_{N+2} satisfying (104), the maximal $d(R_{N+1}, R_{N+2})$ can only be achieved when $R_{N+1} \in \{D_{N+1} - \delta, D_{N+1} + \delta\}$ and $R_{N+2} \in \{D_{N+2} - \delta, D_{N+2} + \delta\}$. To this end, in

order to prove $\cap_{i=1}^2 \mathcal{R}(\boldsymbol{\theta}_{N+i}, \widehat{D}_{N+i}^{(K)}, \delta) \subseteq \mathcal{B}(\boldsymbol{\theta}_T, \Phi(\delta))$, we only need to consider

$$R_{N+1} \in \{D_{N+1} - \delta, D_{N+1} + \delta\}, \quad (112)$$

$$R_{N+2} \in \{D_{N+2} - \delta, D_{N+2} + \delta\}, \quad (113)$$

and show $\boldsymbol{\theta}'_T \in \mathcal{B}(\boldsymbol{\theta}_T, \Phi(\delta))$.

Without loss of generality, we assume that $\boldsymbol{\theta}_{N+1} = \mathbf{0}$, $\boldsymbol{\theta}_{N+2} = (D_S, 0)$, and $\boldsymbol{\theta}_T$ is in the half space above the line passing through $\boldsymbol{\theta}_{N+1}$ and $\boldsymbol{\theta}_{N+2}$. Since $\boldsymbol{\theta}_T \triangleq \mathcal{C}(\boldsymbol{\theta}_{N+1}, D_{N+1}) \cap \mathcal{C}(\boldsymbol{\theta}_{N+2}, D_{N+2})$, we can obtain

$$\begin{cases} x_T^2 + y_T^2 = D_{N+1}^2, \\ (x_T - D_S)^2 + y_T^2 = D_{N+2}^2, \end{cases} \quad (114)$$

which yields

$$\begin{cases} x_T = \frac{D_{N+1}^2 - D_{N+2}^2 + D_S^2}{2D_S}, \\ y_T = \sqrt{D_{N+1}^2 - \left(\frac{D_{N+1}^2 - D_{N+2}^2 + D_S^2}{2D_S}\right)^2}. \end{cases} \quad (115)$$

Similarly, with regard to $\boldsymbol{\theta}'_T = (x'_T, y'_T) = \mathcal{C}(\boldsymbol{\theta}_{N+1}, R_{N+1}) \cap \mathcal{C}(\boldsymbol{\theta}_{N+2}, R_{N+2})$, we also can obtain

$$\begin{cases} x'_T = \frac{R_{N+1}^2 - R_{N+2}^2 + D_S^2}{2D_S}, \\ y'_T = \sqrt{R_{N+1}^2 - \left(\frac{R_{N+1}^2 - R_{N+2}^2 + D_S^2}{2D_S}\right)^2}. \end{cases} \quad (116)$$

By employing (115) and (116), $d(R_{N+1}, R_{N+2})^2$ can be expressed as

$$\begin{aligned} & d(R_{N+1}, R_{N+2})^2 \\ &= \underbrace{\left(\frac{R_{N+1}^2 - R_{N+2}^2 + D_S^2}{2D_S} - \frac{D_{N+1}^2 - D_{N+2}^2 + D_S^2}{2D_S} \right)^2}_{d_x} \\ &+ \underbrace{\left[\sqrt{R_{N+1}^2 - \left(\frac{R_{N+1}^2 - R_{N+2}^2 + D_S^2}{2D_S}\right)^2} - \sqrt{D_{N+1}^2 - \left(\frac{D_{N+1}^2 - D_{N+2}^2 + D_S^2}{2D_S}\right)^2} \right]^2}_{d_y}. \end{aligned} \quad (117)$$

From (112) and (113), d_x can be bounded from above as per

$$\begin{aligned}
d_x &= \left(\frac{R_{N+1}^2 - D_{N+1}^2 + D_{N+2}^2 - R_{N+2}^2}{2D_S} \right)^2 \\
&= \left(\frac{(R_{N+1} - D_{N+1})(R_{N+1} + D_{N+1}) + (D_{N+2} - R_{N+2})(D_{N+2} + R_{N+2})}{2D_S} \right)^2 \\
&\leq \frac{1}{D_S^2} \delta^2 (D_{N+1} + D_{N+2} + \delta)^2 \\
&\leq \frac{1}{D_S^2} (2D_U + \delta)^2 \delta^2
\end{aligned} \tag{118}$$

and moreover, by using the fact that $\sqrt{|x|} - \sqrt{|y|} \leq \sqrt{|x-y|}$ for any x and y , d_y can be bounded from above as per

$$\begin{aligned}
d_y &\leq \left| R_{N+1}^2 - \left(\frac{R_{N+1}^2 - R_{N+2}^2 + D_S^2}{2D_S} \right)^2 - D_{N+1}^2 + \left(\frac{D_{N+1}^2 - D_{N+2}^2 + D_S^2}{2D_S} \right)^2 \right| \\
&\leq |(R_{N+1} - D_{N+1})(R_{N+1} + D_{N+1})| \\
&\quad + \left| \frac{(R_{N+1}^2 - R_{N+2}^2 - D_{N+1}^2 + D_{N+2}^2)(R_{N+1}^2 - R_{N+2}^2 + D_{N+1}^2 - D_{N+2}^2 + 2D_S^2)}{4D_S^2} \right|.
\end{aligned} \tag{119}$$

By employing (112), (113) and (119), we can obtain

$$\begin{aligned}
d_y &\leq \delta (2D_{N+1} + r) + \frac{|R_{N+1}^2 - D_{N+1}^2| + |R_{N+2}^2 - D_{N+2}^2|}{4D_S^2} \\
&\quad \times (|R_{N+1}^2 - D_{N+2}^2| + |R_{N+2}^2 - D_{N+1}^2| + 2D_S^2) \\
&\leq \delta (2D_{N+1} + \delta) + \frac{\delta (2D_{N+1} + \delta) + \delta (2D_{N+2} + \delta)}{4D_S^2} \\
&\quad \times (|(R_{N+1} - D_{N+2})(R_{N+1} + D_{N+2})| + |(R_{N+2} - D_{N+1})(R_{N+2} + D_{N+1})| + 2D_S^2) \\
&\leq \delta (2D_{N+1} + \delta) + \frac{\delta (D_{N+1} + D_{N+2} + \delta)}{D_S^2} \\
&\quad \times [(|D_{N+1} - D_{N+2}| + \delta) (D_{N+1} + D_{N+2} + \delta) + D_S^2]
\end{aligned} \tag{120}$$

$$\begin{aligned}
&\leq \delta (2D_{N+1} + \delta) + \delta (2D_U + \delta) \left[\frac{(D_U - D_L + \delta) (D_{N+1} + D_{N+2} + \delta)}{D_S^2} + 1 \right] \\
&\leq \delta (2D_U + \delta) + \delta (2D_U + \delta) \left(\frac{2D_U + \delta}{D_S} + 1 \right)
\end{aligned} \tag{121}$$

$$\leq (2D_U + \delta) \left(\frac{2D_U + \delta}{D_S} + 2 \right) \delta, \tag{122}$$

where (120) is from (104), and (121) is due to $D_{N+1} \leq D_U$ and Assumption 1 that $D_S > D_U - D_L + 2\Upsilon > D_U - D_L + \delta$, since $\delta < \Upsilon$.

From (117), (118) and (122), we can obtain

$$\begin{aligned}
d(R_{N+1}, R_{N+2})^2 &\leq \frac{1}{D_S^2} (2D_U + \delta)^2 \delta^2 + (2D_U + \delta) \left(\frac{2D_U + \delta}{D_S} + 2 \right) \delta \\
&\leq (2D_U + \delta) \left[\frac{2D_U + \delta}{D_S} \left(\frac{\delta}{D_S} + 1 \right) + 2 \right] \delta \\
&< (2D_U + \Upsilon) \left[\frac{2D_U + \Upsilon}{D_S} \left(\frac{\Upsilon}{D_S} + 1 \right) + 2 \right] \delta,
\end{aligned} \tag{123}$$

which implies

$$d(R_{N+1}, R_{N+2}) < (2D_U + \Upsilon)^{\frac{1}{2}} \left[\frac{2D_U + \Upsilon}{D_S} \left(\frac{\Upsilon}{D_S} + 1 \right) + 2 \right]^{\frac{1}{2}} \sqrt{\delta}, \tag{124}$$

and therefore,

$$\boldsymbol{\theta}'_T \in \mathcal{B}(\boldsymbol{\theta}_T, \Phi(\delta)). \tag{125}$$

Moreover, note that $\mathcal{B}(\boldsymbol{\theta}_T, \delta) \subset \mathcal{R}(\boldsymbol{\theta}_{N+1}, D_{N+1}, \delta)$ and $\mathcal{B}(\boldsymbol{\theta}_T, \delta) \subset \mathcal{R}(\boldsymbol{\theta}_{N+2}, D_{N+2}, \delta)$, and hence $\mathcal{B}(\boldsymbol{\theta}_T, \delta) \subseteq \cap_{i=1}^2 \mathcal{R}(\boldsymbol{\theta}_{N+i}, \widehat{D}_{N+i}^{(K)}, \delta)$. This completes the proof.

APPENDIX B

PROOF OF LEMMA 2

By employing (35) and (51), we can obtain

$$\begin{aligned}
\Phi\left(\frac{3}{2}\delta\right) + \frac{1}{2}\delta &= (2D_U + \Upsilon)^{\frac{1}{2}} \left[\frac{2D_U + \Upsilon}{D_S} \left(\frac{\Upsilon}{D_S} + 1 \right) + 2 \right]^{\frac{1}{2}} \sqrt{\frac{3}{2}\delta} + \frac{1}{2}\delta \\
&< \left\{ (2D_U + \Upsilon)^{\frac{1}{2}} \left[\frac{6D_U + 3\Upsilon}{2D_S} \left(\frac{\Upsilon}{D_S} + 1 \right) + 3 \right]^{\frac{1}{2}} + \frac{1}{2}\Upsilon^{\frac{1}{2}} \right\} \sqrt{\delta} \\
&< \lambda,
\end{aligned} \tag{126}$$

and hence, $\Phi(\frac{3}{2}\delta) < \lambda$.

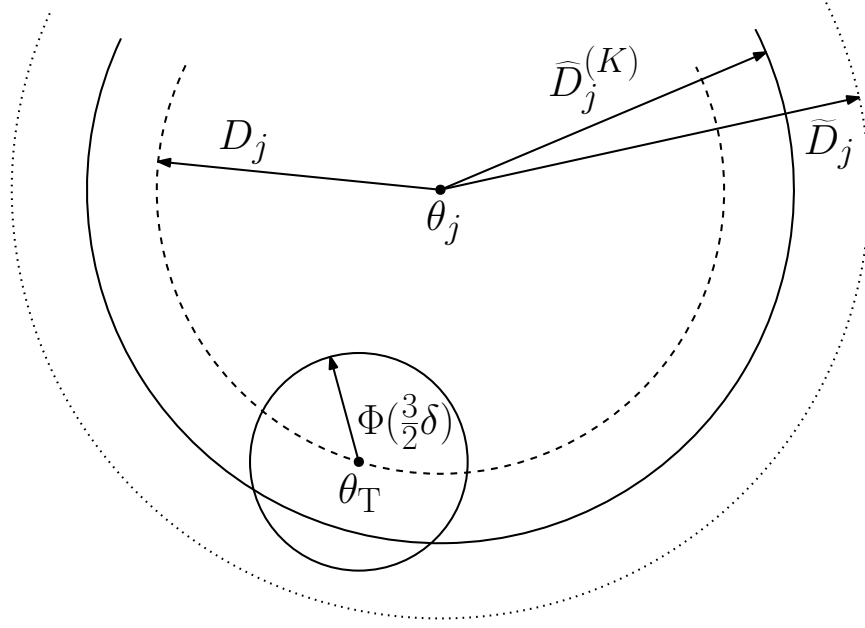


Fig. 15: Geometric illustration of (132).

Furthermore, from (27), (49) and (50), we can obtain that

$$\begin{aligned} |\tilde{D}_j - D_j| &= D_0 P_0^{\frac{1}{\gamma}} \left| \left[\tau_j - F_j^{-1}(\tilde{p}_j(\boldsymbol{\theta}_T)) \right]^{-\frac{1}{\gamma}} - \left[\tau_j - F_j^{-1}(p_j(\boldsymbol{\theta}_T)) \right]^{-\frac{1}{\gamma}} \right| \\ &\geq D_0 P_0^{\frac{1}{\gamma}} \inf_{x \in [\rho_j^{(L)}, \rho_j^{(U)}]} \left| \frac{\partial \left[\tau_j - F_j^{-1}(x) \right]^{-\frac{1}{\gamma}}}{\partial x} \right| |\tilde{p}_j(\boldsymbol{\theta}_T) - p_j(\boldsymbol{\theta}_T)| \end{aligned} \quad (127)$$

$$\begin{aligned} &= D_0 P_0^{\frac{1}{\gamma}} \inf_{x \in [\rho_j^{(L)}, \rho_j^{(U)}]} \left| \frac{\left[\tau_j - F_j^{-1}(x) \right]^{-\frac{\gamma+1}{\gamma}}}{f_j(F_j^{-1}(x))} \right| |\tilde{p}_j(\boldsymbol{\theta}_T) - p_j(\boldsymbol{\theta}_T)| \\ &\geq \frac{\kappa D_0 P_0^{\frac{1}{\gamma}} \left[\tau_j - F_j^{-1}(\rho_j^{(L)}) \right]^{-\frac{\gamma+1}{\gamma}}}{\sup_{x \in [F_j^{-1}(\rho_j^{(L)}), F_j^{-1}(\rho_j^{(U)})]} f_j(x)} \end{aligned} \quad (128)$$

$$> \lambda, \quad (129)$$

where (127) is due to (12) and (22), and (128) is from (23). Thus, we know

$$\mathcal{C}(\boldsymbol{\theta}_j, \tilde{D}_j) \cap \mathcal{B}\left(\boldsymbol{\theta}_T, \Phi\left(\frac{3}{2}\delta\right)\right) = \emptyset, \quad (130)$$

since $\boldsymbol{\theta}_T \in \mathcal{C}(\boldsymbol{\theta}_j, D_j)$ and $\Phi(\frac{3}{2}\delta) < \lambda$.

As illustrated in Fig. 15, if

$$\mathcal{C} \left(\boldsymbol{\theta}_j, \widehat{D}_j^{(K)} \right) \cap \mathcal{B} \left(\boldsymbol{\theta}_T, \Phi \left(\frac{3}{2} \delta \right) \right) \neq \emptyset, \quad (131)$$

then

$$\left| \widehat{D}_j^{(K)} - \widetilde{D}_j \right| \geq \left| \widetilde{D}_j - D_j \right| - \Phi \left(\frac{3}{2} \delta \right), \quad (132)$$

which implies

$$\left| \widehat{D}_j^{(K)} - \widetilde{D}_j \right| \geq \lambda - \Phi \left(\frac{3}{2} \delta \right) > \frac{1}{2} \delta, \quad (133)$$

by employing (126) and (129). Therefore,

$$\mathbb{P}_1 \left(\mathcal{C} \left(\boldsymbol{\theta}_j, \widehat{D}_j^{(K)} \right) \cap \mathcal{B} \left(\boldsymbol{\theta}_T, \Phi \left(\frac{3}{2} \delta \right) \right) \neq \emptyset \right) \leq \mathbb{P}_1 \left(\left| \widehat{D}_j^{(K)} - \widetilde{D}_j \right| \geq \frac{1}{2} \delta \right), \quad (134)$$

which completes the proof.

REFERENCES

- [1] I. Akyildiz, W. Su, Y. Sankarasubramaniam, and E. Cayirci, "A survey on sensor networks," *IEEE Commun. Mag.*, vol. 40, no. 8, pp. 102–114, 2002.
- [2] L. M. Kaplan, Q. Le, and N. Molnar, "Maximum likelihood methods for bearings-only target localization," in *Proc. Int. Conf. Acoustics, Speech, and Signal Processing (ICASSP2001), Salt Lake City, UT, May 2001*, vol. 5, 2001, pp. 3001–3004.
- [3] Y. Shen and M. Z. Win, "Fundamental limits of wideband localization—Part I: A general framework," *IEEE Trans. Inf. Theory*, vol. 56, no. 10, pp. 4956–4980, 2010.
- [4] A. Vempaty, Y. S. Han, and P. K. Varshney, "Target localization in wireless sensor networks using error correcting codes," *IEEE Trans. Inf. Theory*, vol. 60, no. 1, pp. 697–712, 2014.
- [5] R. Niu and P. K. Varshney, "Target location estimation in sensor networks with quantized data," *IEEE Trans. Signal Process.*, vol. 54, no. 12, pp. 4519–4528, 2006.
- [6] O. Ozdemir, R. Niu, and P. K. Varshney, "Channel aware target localization with quantized data in wireless sensor networks," *IEEE Trans. Signal Process.*, vol. 57, no. 3, pp. 1190–1202, 2009.
- [7] A. Vempaty, O. Ozdemir, K. Agrawal, H. Chen, and P. K. Varshney, "Localization in wireless sensor networks: Byzantines and mitigation techniques," *IEEE Trans. Signal Process.*, vol. 61, pp. 1495–1508, 2013.
- [8] Z. Li, W. Trappe, Y. Zhang, and B. Nath, "Robust statistical methods for securing wireless localization in sensor networks," in *Proc. Int. Workshop Inf. Process. Sens. Netw.*, April 2005, pp. 91–98.
- [9] J. H. Lee and R. M. Buehrer, "Characterization and detection of location spoofing attacks," *J. Commun. Netw.*, vol. 14, no. 4, pp. 396–409, 2012.
- [10] S. Cui, Z. Han, S. Kar, T. T. Kim, H. V. Poor, and A. Tajer, "Coordinated data-injection attack and detection in the smart grid: A detailed look at enriching detection solutions," *IEEE Signal Process. Mag.*, vol. 29, no. 5, pp. 106–115, 2012.
- [11] A. Vempaty, L. Tong, and P. Varshney, "Distributed inference with Byzantine data: State-of-the-art review on data falsification attacks," *IEEE Signal Process. Mag.*, vol. 30, no. 5, pp. 65–75, 2013.
- [12] J. Zhang, R. S. Blum, X. Lu, and D. Conus, "Asymptotically optimum distributed estimation in the presence of attacks," *IEEE Trans. Signal Process.*, vol. 63, no. 5, pp. 1086–1101, March 2015.

- [13] B. Alnajjab, J. Zhang, and R. S. Blum, "Attacks on sensor network parameter estimation with quantization: Performance and asymptotically optimum processing," *IEEE Trans. Signal Process.*, vol. 63, no. 24, pp. 6659–6672, 2015.
- [14] J. Zhang and R. S. Blum, "Distributed joint spoofing attack identification and estimation in sensor networks," in *Proc. IEEE China Summit Int. Conf. Signal Inf. Process.*, 2015, pp. 701–705.
- [15] J. Zhang, R. S. Blum, L. M. Kaplan, and X. Lu, "Functional forms of optimum spoofing attacks for vector parameter estimation in quantized sensor networks," *IEEE Trans. Signal Process.*, vol. 65, no. 3, pp. 705–720, 2017.
- [16] A. Boukerche, H. Oliveira, E. F. Nakamura, and A. A. Loureiro, "Secure localization algorithms for wireless sensor networks," *IEEE Commun. Mag.*, vol. 46, no. 4, pp. 96–101, 2008.
- [17] L. M. Huie and M. L. Fowler, "Strategies for information injection for networks estimating emitter location," *IEEE Trans. Aerosp. Electron. Syst.*, vol. 51, no. 3, pp. 1597–1608, 2015.
- [18] S. Capkun and J.-P. Hubaux, "Secure positioning in wireless networks," *IEEE J. Sel. Areas Commun.*, vol. 24, no. 2, pp. 221–232, 2006.
- [19] W. T. Zhu, Y. Xiang, J. Zhou, R. H. Deng, and F. Bao, "Secure localization with attack detection in wireless sensor networks," *Int. J. Inf. Secur.*, vol. 10, no. 3, pp. 155–171, 2011.
- [20] A. Dembo and O. Zeitouni, *Large Deviations Techniques and Applications*, 2nd ed. New York, NY, USA: Springer-Verlag, 2009.